Thesis for Master's Degree

Microstructure-based Modeling of Coated Surfaces

Mijanur Rahaman Chowdhury

School of Information and Mechatronics

Gwangju Institute of Science and Technology

Gwangju, Republic of Korea

July, 2007

Microstructure-based Modeling of Coated Surfaces

Advisor: Professor Kwan Heng Lee

by

Mijanur Rahaman Chowdhury

School of Information and Mechatronics

Gwangju Institute of Science and Technology

Submitted to the School of Information and Mechatronics in partial fulfillment of the requirements for the degree of Master of Science at the Gwangju Institute of Science and Technology.

Gwangju, Republic of Korea
June 15, 2007
Approved by

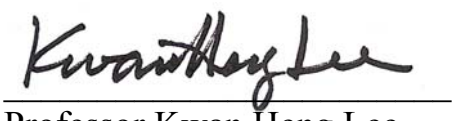

Professor Kwan Heng Lee
Thesis Advisor

Microstructure-based Modeling of Coated Surfaces

Mijanur Rahaman Chowdhury

Accepted in partial fulfillment of the requirements
for the degree of Master of Science

June 15, 2007

Thesis Advisor
Prof. Kwan Heng Lee

Committee Member
Prof. Yong Gu Lee

Committee Member
Prof. Kwang Hee Ko

MS/SIM
20054181

Mijanur Rahaman Chowdhury. **Microstructure-based Modeling of Coated Surfaces**. School of Information and Mechatronics. 2007. Advisor: Professor Kwan Heng Lee.

Abstract

The appearance of real-world materials is the result of complex interaction of the light incident on the object, human perception, and the optical reflectance properties of the material. The optical reflectance properties of a coating material depend on its surface topography and the composition of its subsurface microstructure. Among other factors, the composition of its microstructure plays the major role in determining the final appearance of a coated surface. Therefore, the identification and characterization of the microstructure of coating materials are crucial for predicting the appearance of materials.

In this thesis, we attempt to relate the appearance of coated surfaces to the composition of their microstructures by microstructure-based modeling of the appearance. We first conduct a series of studies on coated materials having various controlled microstructural properties such as pigment size, pigment density and so on. We then use a hybrid method that incorporates both the analytical model and the acquired reflectance data from a series of samples varying their microstructural properties to approximate their reflectance. Several existing reflection models are used to fitting the measured reflectance data by the nonlinear optimization technique to determine the appropriate parameters of the models for these samples.

Using the measured data and fitted parameters, we then render various coated surfaces having different composition of microstructure on a hardware-accelerated rendering system. Comparison is also performed between the measured and the BRDF model's rendering results. In addition, we analyze several well-known BRDF models in terms of their ability to approximate the appearance of coated materials based on the fitting result. We believe this work can serve as a guide for developing a simple and easy-to-use reflection model for predicting the appearance of coated surface from their compositions of microstructure.

Dedicated to the two invaluable persons in my life
My nana and nani
(Mr. and Mrs. A. Q, Chowdhury)

Acknowledgment

First and foremost, I would like to thank and express my heartfelt gratitude to my advisor, Professor Kwan Heng Lee, for the support and encouragement he gave me during my stay at GIST. His constant confidence in me and my work has been an inspiration which propelled me to try to think and work harder. Working with him has been a fruitful and enjoyable learning experience. I would also like to thank Professor Kwanghee Ko, whom I enjoyed working for couple of months. Thank also goes to my thesis committee member Professor Yong Gu Lee for his insightful input and comment which helped me to modify some portion of my thesis.

During my time in the Intelligent Design and Graphics group, I had the pleasure of working with many wonderful people. I thank my research group leader Kang Yeon Kim for his help from the very beginning of my research. He taught me a great deal about rendering and other topics of computer graphics. His rendering code is responsible, one way or another, for every rendered image in this dissertation. Without the many valuable discussion and suggestions from Hoe Min Kim, this dissertation would not be what it is. He also provided me the BRDF parameterization code. Thanks to Hyun Jin Yoo for her relentless help and support during my work. Myoung Kook Kim helped extensively with my BRDF measurement. Thank also goes to Kang Su Park and Seung Joo Lee who also measured few coated sample for me. I also would like to thank Wojciech Matusik of Mitsubishi Electric Research Laboratory (MERL) for providing me the access to his well-known BRDF database.

Many thanks to my seniors – Joung Wook Park, Eu Cheol Kang, Kim Hyun Soo, Duck-Bong Kim for their assistance and advice. Special thanks to Seung Man Kim, Han Kyun Choi, Ji Ho Cho, Sun Uk Hwang, Je Hoon Song, Ja Yong Lee and In Yeob Chang for their extensive help on different occasions. I would like to convey my gratitude and thanks to Jae Doug Yoo, who was always supportive and also helped me extensively in applying for scholarship and in other occasions.

Last but not the least, I owe the deepest gratitude to my parents, brothers, my younger sister and friends for their invaluable support. Their constant encouragements are what keep me going.

Table of Contents

Front Matter

Chapter 1. Introduction

Chapter 2. Background

Chapter 3. Coating or Paint Microstructure

Chapter 4. Microstructure-based Modeling

Chapter 5. Results and Discussion

Chapter 6. Conclusions and Future Work

List of Figures

List of Tables

Chapter 1

Introduction

For much of its history, modeling the appearance of real-world materials has been a major focus in the study of computer graphics. Researchers have pursued the stronger goal of modeling the appearance of various classes of materials. While some materials' appearances are quite easy to simulate because of their simple light interaction properties, several classes of materials remain difficult to reproduce, most notably human skin, fabrics and coated surface. This thesis focuses on one of the latter classes of material i.e. modeling the appearance of coated surfaces.

Moreover, in this world of global competition, products developed by different industries are often of similar quality and functionality, and the appearances of these products often determine commercial success. Therefore, different types of coating are the popular choices among the makers because of their ability to increase the richness of visual effects of a surface. Nowadays, paint or coating can be found on almost everything – from kitchen appliances to clothing and it is also claimed that almost eighty percent of all automobiles have metallic finishes. Therefore, simulation of product's appearance with coatings becomes of primary importance.

The first step to model the appearance of any material is to perceive which factors govern its appearance. The visual appearance of a real-world object is usually governed by reflectance properties with its geometric components, namely different components of microstructure. The microstructure level involves surface micro facets that are visually indistinguishable. Some materials like smooth metals, plastics have very simple microstructure level i.e. only composed of one layer and hence easy to simulate the appearance.

On the other hand, several classes of material have very complex microstructure and thus difficult to reproduce. Paint or coating is one of them which are normally composed of two layers with different types of visually indistinguishable components. The reflection properties of the painted surface depend on the composition of its microstructure. In other words, the light

interaction properties with visually indistinguishable components of its microstructure plays major role in determining the final appearance of the coated surfaces.

Since the appearance of coating material depends on the composition of paint's microstructure, we first conduct a series of studies on the subsurface microstructure and their various component of coating. Traditionally, paint consists of two layers called clearcoat and basecoat. The basecoat usually consists of many components and various composition of basecoat makes different paint. A detail description of the composition of coating or paint is presented in chapter 3.

The light interaction properties of materials are commonly expressed by a function called Bidirectional Reflectance Distribution Function (BRDF). BRDF describes how light interacts at a surface point. It is a function of the incoming and outgoing directions that describes how much of the incoming light is reflected. The BRDF can fully describe the appearance of homogeneous materials e.g. most plastic and smooth metals. To model the appearance of paint, we need to determine the BRDF of it. Even if the rendering equation is solved exactly, inaccurate BRDFs will lead to an incorrect image. There are mainly two ways to determine BRDFs of a surface: direct measurement and analytical BRDF models.

BRDFs of a surface are usually measured by a traditional device called gonio-reflectometer. Recently, image-based measurement system, proposed by Marchener et al. [19], becomes popular. Though direct exhaustive measurement of real materials is a viable alternative for materials that are difficult to model, its use is far from widespread due to high cost of measurement times and equipment setup.

Another way to determine BRDFs of a surface is to use analytical reflection models. Analytical reflection models are usually very simple and easy to use. Over the past few decades, numerous analytical BRDF models have been proposed for improved fidelity, flexibility and computation efficiency. A brief overview of the popular existing analytical BRDF models is provided in chapter 2. However, selecting a BRDF model from these wide ranges of models and choosing the appropriate parameter values which faithfully represent the reflection properties of a real world surface is a difficult task. A simple model will allow for easy parameter selection but often will result in an inaccurate representation. On the other hand, a complex model offers the

ability to represent a wide variety of surfaces but the correct selection of parameter values can be daunting.

Since both of the approaches described above have advantage and disadvantage as well, we follow a hybrid approach to determine BRDFs of coated surfaces. We, at first, collect samples coated with paint of varying composition of microstructure. A description on our samples is presented in chapter four. We then measure the BRDFs of the samples using our image-based BRDF acquisition system. Analytical BRDF models are then used to fit to the measured BRDF using nonlinear least square optimization technique to determine the appropriate parameters of the models and select the best reflection model for that surface. Applying hybrid approach has the following purposes: it helps us to select the best reflection model with faithful parameters for that surface and it also can serve as a guide for those who wants to render painted surfaces accurately with easy-to-use analytic BRDF models without spending time on extracting BRDF data from exhaustive measurement by gonio-reflectometer from real paint sample. After extracting the parameters of analytical BRDF models, we render coated surfaces with various composition of microstructure taking the use of graphics processing unit (GPU) features to accelerate rendering for relating the appearance of coating with its microstructure composition which is presented in chapter five.

1.1 Thesis Contribution

The work presented in this thesis tackles a number of issues in microstructure-based coating appearance simulation. In more detail, the main contribution of thesis is as follows:

- A series of studies on the subsurface microstructure of coated surfaces and the influence of the constituents on the appearance of the surfaces based on a series of studies.

- Analysis of several well known BRDF models in terms of their ability to approximate the reflectance of coated surface by fitting those models to real reflectance data measured by image-based measurement system proposed by Marschener et al. [19].

- Determination of best analytic BRDF model among the wide range of existing model which can best approximate the reflectance of coated surfaces.

- Analysis of the effect of major microstructural component on the appearance of coated surface.

- Modeling the appearance of the coated surface based on their composition of microstructure. Simulating the appearance using the measured reflectance data as well as various BRDF models to evaluate the capability of the models to approximate the appearance of the coated surfaces varying in their composition of microstructure.

1.2 Thesis Overview

The rest of this thesis is structured as follows: In chapter 2, we introduce the fundamental concept and terminology in the field of material appearance and provide a broad overview of BRDF models and its measurement system. We describe the composition of paint and its microstructure in chapter 3. In chapter 4, we present the overall process on microstructure-based modeling of coating. We also review previous works on paint appearance simulation in this chapter. Chapter 5 outlines the results and discussions of modeling process described in chapter. 4. Finally, we conclude the thesis and provide directions for future work in chapter 6.

Chapter 2

Background

The central theme of modeling the appearance of any material is to perceive how light interact with it. The image we perceive if we look at an object depends on a whole series of effects of light on this object: light emitting from light source to finally reaching to an observer's eye after illuminating it. This chapter of this thesis gives an overview on underlying physics of light, light interaction with matter and appearance representation. At first, we describe models of light, nomenclatures of reflectance i.e. basic radiometric and photometric quantities, interaction of light and matter and appearance representation functions. We next describe how reflectance or BRDF can be defined by these nomenclatures. Finally, we briefly review BRDF, its properties, analytic BRDF models and image-based measurement of BRDF and data processing after measurement. Most of the descriptions presented in this chapter are adapted from [10], [14] [16], [18], [20] and [23].

2.1 Models of Light

The nature and various properties of light, its interaction with various materials, and the reception of light by either the human visual system or by an imaging system are few fundamental aspects of computer graphics, appearance modeling and computer vision.

In general, the study of light has three sub-fields: physical optics, geometric optics and quantum optics. Physical optics is concerned with the study of the wave nature of light. The particle nature of light is the topic of geometric optics. Quantum optics deals with the study of the dual wave-particle nature of light and attempts to construct unified theories to support duality.

Computer graphics are mostly concerned with geometric optics but need some of the others too. For example, reflection and refraction of light are mostly described by thinking as light as particles like in geometric optics. On the other hand, color is fundamentally described in terms of waves, which is dealt in physical optics.

2.2 Radiometry and Photometry

Radiometry is the measurement of electromagnetic energy and covers a wide range of wavelengths including infrared, visible and ultraviolet light. On the other hand, photometry covers only the visible spectrum and takes the sensitivity of the human visual system into account. In other words, photometry is the perceptual analog of radiometry where all measurements are relative to perception. We in this section define the most important radiometric and photometric terms and then use them to describe the reflection of light in later sections. In computer graphics light transport is mostly simulated at the geometric optics level. Wave phenomena like diffraction and interference are typically ignored with little exception. In this thesis, we also ignore effects of polarization, fluorescence and phosphorescence.

2.2.1 Radiometric Quantities

The following description of radiometric quantities is provided for the whole spectrum but these quantities can also be evaluated for a specific wavelength lambda, λ .The unit of a spectral term is the unit of the corresponding radiometric term divided by the unit of length [m].

Radiant Energy, Q

This is the basic quantity that describes the energy transported by light of all wavelengths measured in Joule [J].

Radiant Flux, Φ

Radiant flux or electromagnetic flux, often denoted by Φ, expresses the radiant energy per unit time or power of the radiation. The unit of radiant flux is Watt [W].

$$\text{Radiant flux, } \Phi = \frac{dQ}{dt}$$

Radiant Exitance or radiosity, B

Radiant exitance or radiosity, denoted by B, is the radiant flux per surface area exitant from a point of a surface. The unit of radiant exitance is Watt/meter^2 [W/m^2].

$$\text{Radiant exitance, } B = \frac{d\Phi}{dA}$$

Irradiance, E

This quantity, denoted by E, is defined as the flux per unit surface area and is often used to describe the amount of energy striking the surface from a certain direction. Irradiance is very similar to radiosity, but it measures the incident light rather than exitant light. It is defined for all directions *w*:

$$\text{Irradiance, } dE(w) = \frac{d\Phi}{dA}$$

It can also be obtained by integrating the radiance over the solid angle. The unit of irradiance is Watt/meter^2 [W/m^2].

Radiant Intensity, I

While radiosity or irradiance is defined as surface density of flux at a point, radiant intensity, denoted by the letter I, is the directional density of flux in a given direction which is defined as radiant flux per solid angle. A solid angle is a 3D analog to the familiar 2D concept of an angle which represents the subtended surface area when the region is projected to the unit sphere. Radiant intensity is particularly relevant when examining a very distant or very small light source. The unit is Watt/steredian [W/sr].

$$\text{Radiant intensity, } I = \frac{d\Phi}{d\omega}$$

Radiance, L

This is the most fundamental concept in radiometry. It is a physical quantity equivalent to the psychological concept of brightness observed by humans. In other words, it is exactly what is perceived by an observer – be it a human eye or an electronic device – and is therefore one of the most important quantity for image-based modeling. It is measured in radiant flux per unit projected area per unit solid angle. Radiance has the important property of being constant along a ray in empty space. This is the inherent reason for the fact that the signal seen by an imaging system is independent of the distance to the object.

On the rendering side, radiance is (at least implicitly) used by most rendering system such as ray tracing. Mathematically,

$$\text{Radiance, } L = \frac{d^2\Phi}{dA_{proj}\,dw} = \frac{d^2\Phi}{dA\cos\theta\,dw}$$

Where,

dw = is the solid angle

$dA_{proj} = dA\cos\theta$ = projected area

θ = angle between the outward surface normal of the area element dA and the direction of observation.

2.2.2 Photometric Quantities

Photometry is the psychophysical measurement of light which is detectable by the human eye. It is thus restricted to the wavelength range from about 380 to 780 nm. In other words, the only difference between radiometry and photometry is that radiometry includes entire optical radiation spectrum, while photometry is limited to the visible spectrum as defined by the response of the eye.

Definition	**Radiometric Quantity**	**Radiometric Unit**	**Photometric Quantity**	**Photometric Unit**
Energy	Radiant Energy	Joule [J]	Luminous Energy	[*talbot*]
Power	Radiant Flux	Watt [W=J/s]	Luminous Flux	lumen [lm = talbot/s]
Power per unit area	Irradiance or Radiosity	[W/m^2]	Illuminance Luminosity	lux [lx = lm/m^2]
Power per unit solid angle	Radiant Intensity	Watt/steredian [W/sr]	Luminous Intensity	candela [cd = lm/sr]
Power per area per solid angle	Radiance	[W/(m^2.sr)]	Luminance	[nit = cd/m^2]

Table 2.1: Basic radiometric quantities and their photometric counterparts.

Each photometric quantity can be computed from the corresponding spectral radiometric quantity by convolving it with the spectral efficiency function V(λ). For example, luminosity B_v, the photometric quantity corresponding to radiosity of radiometry, is defined as:

$$B_v = \int B_\lambda . V_\lambda . d\lambda$$

Table 2.1 summarizes and compares radiometric and photometric quantities and their units.

2.3 Interaction of Light and Matter

The interaction of light and matter is a complex physical process. Among various aspect, one of the most important topics of this process is to perceive how light behaves when it strikes a material boundary i.e. physics of light reflection and refraction. The following section describes the underlying physical principles of this process.

Physics of Reflection and refraction

When light strikes a material boundary, for example, crossing from air into glass, some of the light transmits into the new material; some light reflects at the boundary. This behavior of light is mainly determined by the indices of refraction of the two materials. The direction of reflected and transmitted ray can be computed from Snell's law and Fresnel equation determines the amount of refracted and reflected flux.

The following figure depicts this scenario where a ray traveling through a material with refractive index, n_1 and strikes another material of refractive index, n_2. The indices of refraction, n_λ is defined as the ratio of the speed of light in a material, v_λ to the speed of light in vacuum, c.

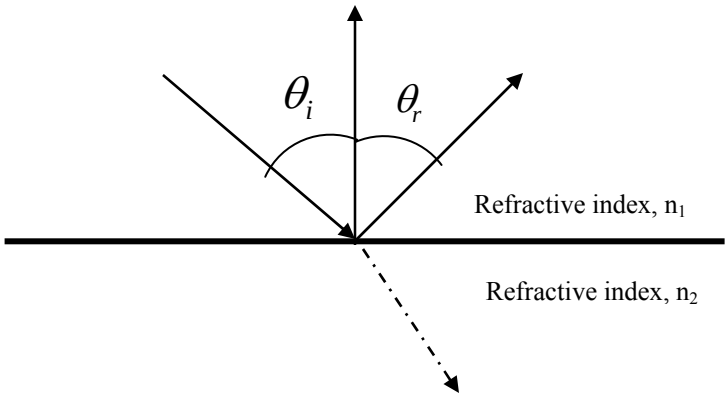

Figure 2.1: Physics of light reflection and refraction

Snell's Law

Snell's law is used to describe the relationship between the angle of incidence and the refraction. It states that the relationship between the refracted angle, θ_t between the surface normal, **n** and the transmitted ray **t** and the incident angle, θ_i :

$$n_1 \sin\theta_i = n_2 \sin\theta_t$$

The angle θ_r between the reflected ray **r** and the surface normal, **n** is equal to θ_i :

$$\sin\theta_i = \sin\theta_r$$

Fresnel Equations

The Fresnel's formula, deduced by *Augustin-Jean Fresnel*, describes how much light reflects when moving between media of differing refractive indices. The reflection of light that the equation predicts is known as Fresnel reflection.

The fraction of the intensity of incident light that is reflected from the interface is given by the reflection coefficient, R and the fraction refracted by the transmission coefficient, T. The calculation of R and T depend on polarization of the incident ray. If the light is polarized with the electric field of the light perpendicular to the plane of incidence, the reflection coefficient is given by:

$$R_s(\theta) = \left[\frac{\sin(\theta_t - \theta_i)}{\sin(\theta_t + \theta_i)}\right]^2 = \left[\frac{n_1\cos\theta_i - n_2\cos\theta_t}{n_1\cos\theta_i + n_2\cos\theta_t}\right]^2$$

If the incident light is polarized parallel to the plane of incidence, the R is given by:

$$R_p(\theta) = \left[\frac{\tan(\theta_t - \theta_i)}{\tan(\theta_t + \theta_i)}\right]^2 = \left[\frac{n_1\cos\theta_t - n_2\cos\theta_i}{n_1\cos\theta_t + n_2\cos\theta_i}\right]^2$$

where , θ_t can be computed from , θ_i using Snell's law.

The transmission coefficient in each case is given by:

$$T_s(\theta) = 1 - R_s(\theta)$$
$$T_p(\theta) = 1 - R_p(\theta)$$

If the incident light is unpolarized, the reflection coefficient, R is given by:

$$R(\theta) = \frac{R_s(\theta) + R_p(\theta)}{2}$$

Schlick [31] proposed a good approximation to the Fresnel reflection coefficient for unpolarized light based on the *Fresnel reflection coefficient* at normalized incidence R(0):

$$R(\theta) \approx R(0) + [1 - R(0)][1 - \cos\theta]^5$$

2.4 Representation of Appearance

It is possible to describe the interaction of light and matter entirely using their physical interaction principles such as Snell's law or the Fresnel equations described in previous sections. Alternatively, we can observe the actual interaction using suitable techniques and derive models that reflect this principle of interaction of light with matter. This section presents several functions that can describe light interaction with materials of different light interaction properties which are the basis for the simulation of their appearance. This section's description is adapted from [14] [32].

2.4.1 Taxonomy of appearance representation

When a photon of light strikes a surface, there are possible six parameters for each of striking photon and resulting photon that leaves the surface to describe the light interaction characteristics of the surface. The parameters are: x, y, t, θ, Φ and λ for each photon of light. The first two parameters denote position of the photon. Parameters θ and Φ represent the spherical coordinate of the incident ray of photon. Parameters, t and λ, denotes time and wavelength respectively. We see that in order to characterize the behavior of a surface, we need a function that gives the amount of reflected light for each possible value of these 12 parameters, shown below:

$$(x, y, t, \theta, \Phi, \lambda)_{in} \rightarrow (x, y, t, \theta, \Phi, \lambda)_{out}$$

But dealing with this 12-parameter function is not really possible. That is why assumption is usually made to simplify it further. Figure 2.2 shows the simplification process.

The following section describes some special function which we will come across in the process of simplification of 12-parameter function and these functions are of more importance than others in appearance modeling.

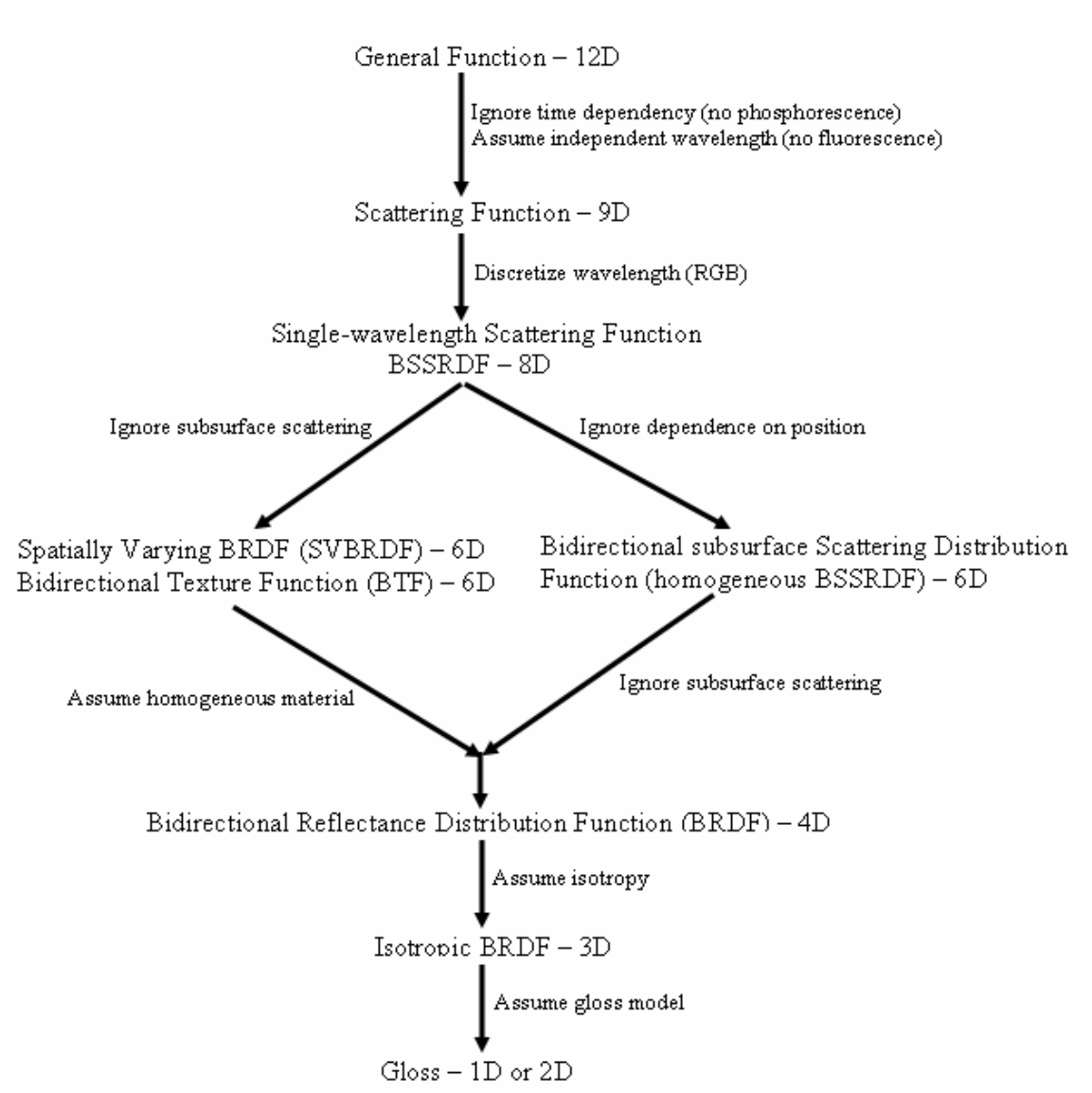

Figure 2.2: Taxonomy of appearance representation (image adapted from [34])

Generalized scattering function

Let us start with the original 12D space. We can eliminate a dimension by assuming that we do not have phosphorescence. That is, the light reflected immediately after it strikes the surface, meaning that $t_{in} = t_{out.}$ We can also assume that the appearance of the surface is constant over time, permitting us to eliminate both time variables completely.

Next, we can assume that there is no fluorescence, meaning the incoming wavelength is equal to the outgoing wavelength, meaning that $\boldsymbol{\lambda_{in} = \lambda_{out}}$. The 9D function resulting from these simplifications is called a generalized scattering function.

BSSRDF

In typical computer graphics and computer vision applications, the wavelength is normally discretized. Three band called red, green and blue are typically used since the human eye only has three kinds of receptors. This phenomenon helps us to get rid of another dimension giving an 8-dimensional function called Bidirectional Surface Scattering Distribution Function (BSSRDF). BSSRDF, generally denoted by S, defined as the ratio of reflected radiance dL_r in the direction (θ_r , Φ_r) at a point (x_r , y_r) to incident flux $d\Phi_i$ coming from direction (θ_i , Φ_i) at a point (x_i , y_i):

$$S(\theta_i, \Phi_i, x_i, y_i, \theta_r, \Phi_r, x_r, y_r) = \frac{dL_r(\theta_r, \Phi_r, x_r, y_r)}{d\Phi_i(\theta_i, \Phi_i, x_i, y_i)}$$

It provides a general model of light transport inside an object and often used to model the light transport in scattering material such as skin, wax or marble. It is a very general property of a surface and captures all kinds of light transport, including subsurface scattering. However, the high-dimensionality of the BSSRDF makes it very difficult to measure and use. As a result, it is often reduced to simpler representations by imposing certain assumptions or restrictions.

BTF and SVBRDF

From this 8-dimensional function space, we can make two different simplifications. First, we can ignore the presence of subsurface scattering. That is, we assume that $(x, y)_{in} = (x,y)_{out}$ resulting in a six dimensional function.
We may think of this function in two ways: it is either a texture map that varies with illumination and viewing direction (thus a Bidirectional Texture Function or BTF) or a BRDF that varies with (x, y) position on the surface (thus spatially-varying BRDF or SVBRDF).

For this dissertation, the main function we will consider is the BRDF. Referring to the taxonomy, we see that the BRDF is a special case of BTF or spatially-varying BRDF assuming no variation across the surface. In the following few sections, we will present a brief overview of BRDF, its properties and representation and BRDF measurement system.

2.5 BRDF

The Bidirectional Reflectance Distribution Function or BRDF which was first defined by *F. Nicodemus et al.* [24] in 1970 deals with the light that is immediately reflected when reaching the surface. This function is used in a number of areas like in image processing, including pattern recognition and remote sensing, and also in computer graphics for rendering realistic looking images. It is a generalization of BSSRDF which does not consider light that scatter inside the material and then leaves. This simplification takes advantage of the observation that, for most materials, the radiant flux incident at a point emerges from a point very near the point of incidence. BRDF is a function of four variables: two variables specify the incoming light direction; two other variables specify the outgoing light direction as shown in figure 2.3. It is defined as the ratio of outgoing radiance, $dLr(\theta_r, \Phi_r)$ to the incoming irradiance $dE_i(\theta_i, \Phi_i)$:

$$f_r(\theta_i, \Phi_i, \theta_r, \Phi_r) = \frac{dL_r(\theta_r, \Phi_r)}{dE_i(\theta_i, \Phi_i)} = \frac{dL_r(\theta_r, \Phi_r)}{L_i(\theta_i, \Phi_i)\cos\theta_i d\omega_r}$$

The unit of BRDF is $\frac{1}{steredian}[\frac{1}{sr}]$.

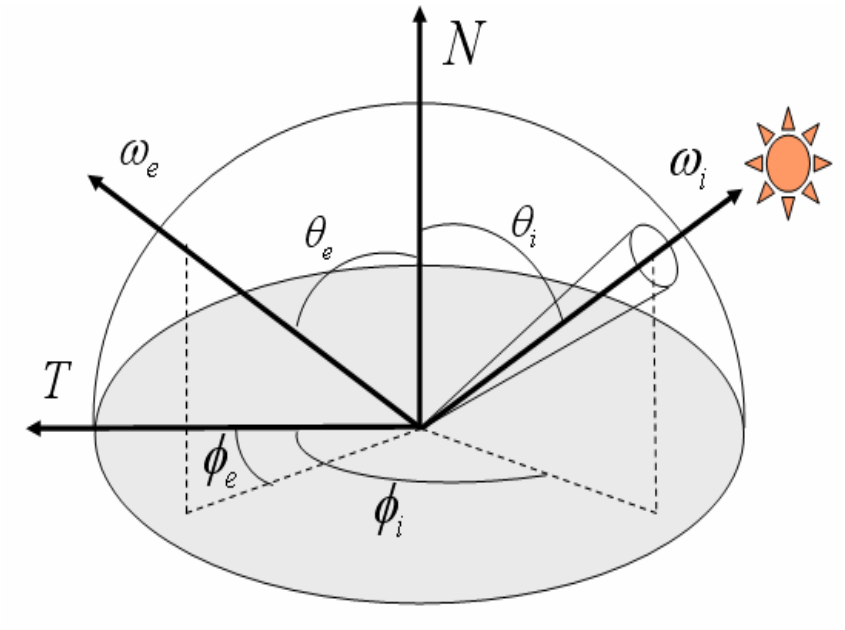

Figure 2.3: BRDF coordinate system.

2.6 Properties of BRDF

There are some basic principles of physics which a BRDF must fulfill to be physically plausible. The most important of these are as follows:

Non-negativity

The first property is non-negativity which states that all values of function, f_r must be non-negative. In fact, they can be any value from the interval [0, ∞]. This is because both radiance and irradiance must be non-negative.

Reciprocity

This property, called as *Helmholtz's law of reciprocity*, must be satisfied by a BRDF to make it physically valid. It states that the surface reflectance should be independent of the direction of the light flow – if the flow of light is reversed the value of the BRDF should be the sane. This means that swapping the incoming and outgoing directions should yield the same value of f_r :

$$f_r(\theta_i,\Phi_i,\theta_r,\Phi_r) = f_r(\theta_r,\Phi_r,\theta_i,\Phi_i)$$

Energy Conservation

In order to physically plausible, a BRDF must fulfill energy conservation rule which states that a BRDF must not reflect more energy than it receives. In other words, the amount of energy that is received by the surface element from some specific direction must be greater than the sum of the energy emitted by the surface element in all possible directions. This must be true for the energy received from all possible directions. The underlying assumption is that the surface element does not emit the energy by itself (e.g. the surface is not fluorescent). Mathematically,

$$\int_{\Omega} f_r(\theta_i, \Phi_i, \theta_r, \Phi_r) \cos\theta_o \, d\omega_o \leq 1$$

2.7 Isotropic BRDF

One of the important subclass of four-dimensional BRDF is three-dimensional isotropic BRDF. This isotropic BRDF is valid for materials in which rotations about the surface normal can be ignored. It means that the reflectance is the same when the material sample is rotated about the normal while the directions of the incoming irradiance and outgoing radiance are fixed. This BRDF property is shared by many materials especially whose have no "grain" or distinguished direction to its material. That is, for an isotropic surface:

$$f_r(\vec{\omega}_i, \vec{\omega}_e) = f_r(R\vec{\omega}_i, R\vec{\omega}_e)$$

where $\omega_i \, and \, \omega_e$ are incident and outgoing light vector and R is any rotation about the surface normal (figure 2.4).

Formally, a BRDF, f_r is isotropic if,

$$f_r(\theta_i, \Phi_i, \theta_0, \Phi_0) = f_r(\theta_i, \Phi_i + \varphi, \theta_0, \Phi_0 + \varphi)$$

and,

$$f_r(\theta_i, 0, \theta_0, 0) = f_r(\theta_i, 0, \theta_0, -\Phi_0)$$

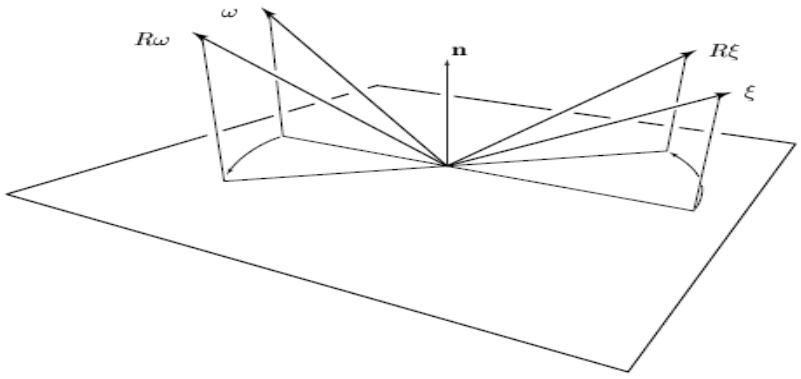

Figure 2.4: Rotating a configuration about the surface normal. For an isotropic BRDF, $f_r(\omega_i, \xi) = f_r(R\omega_i, R\xi)$. (Image from [18])

Isotropic BRDF can be written as a function of 3 variables. The variables Φ_o and Φ_i can be replaced by one variable $\Phi_{diff} = (\Phi_o - \Phi_i)$. Therefore, the coordinate system of isotropic BRDF is shown in figure 2.5.

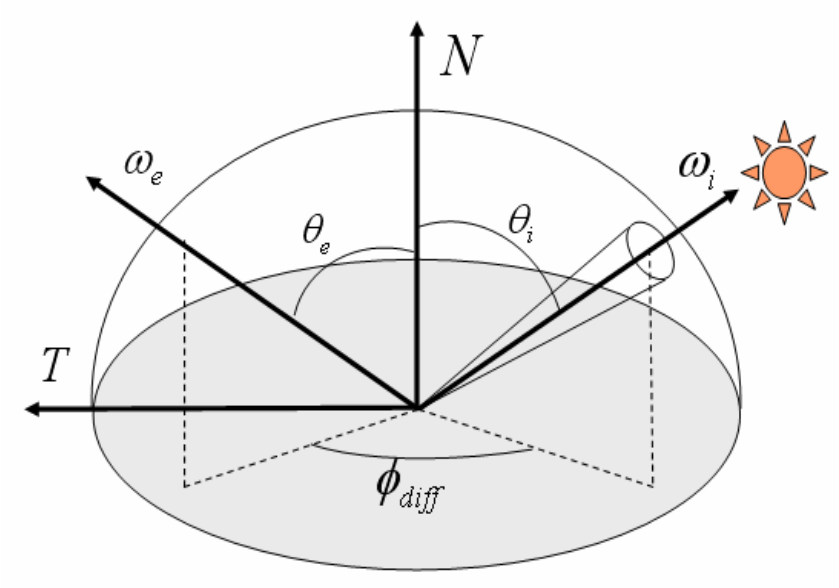

Figure 2.5: Isotropic BRDF coordinate system

However, anisotropic surfaces cannot be modeled using isotropic BRDFs that are parameterized using only three variables. Anisotropic surfaces have microgeometry with strongly oriented elements. The orientation of these elements causes the light to reflect in preferred directions relative to the local coordinate system expressed by tangent, normal, and binormal. A distant observer does not see the microstructure, but instead only its effect on the reflected light. However, for the vast majority of the natural and man-made surfaces the microgeometry is randomly distributed and doesn't have any preferred direction.

2.8 Analytic BRDF Model

Among the variety of basic strategies for modeling BRDFs of a surface in both the field of computer graphics and computer vision, the most simple and widely used method is analytic BRDF model. A BRDF model is typically composed of two components, the diffuse term and the specular term. The diffuse term generally describes the aggregate effects of multiple reflections. As a result, it is mostly independent of the light and view direction. In the ideal case it is lambertian, i.e. constant for all direction pairs. The specular term generally describes the directional component of reflection. For common materials which are not entirely diffuse, the overall reflection for a particular incident ray has a maximum near the mirror direction. The specular term specifies the location of this peak, together with the falloff surrounding it. There are wide ranges of BRDF models available which can be roughly divided into two classes: phenomenological models and physically-based model. A number of well-known phenomenological and physically based models will be listed here. We change the notations of the models from their original form for more consistent notation. For further information on the models, the reader is referred to the original papers. In all models presented below, we enforce the diffuse term to be lambertian. In table, the common notations we use are listed.

Common notation	
K(**L**,**V**) : BRDF evaluated at (**L**, **V**)	**H** : Half-way vector between L and V
L : Incoming vector (light)	θ_h : Angle between N and H
V : Outgoing vector (view)	F : Fresnel value
N : Normal	D : Microfacet distribution
G : Geometric Factor/Roughness Term	K_d : diffuse lobe scaling factor
R : Reflection vector (mirror)	K_s : specular lobe scaling factor

Table 2.2: Common notation for BRDF models

2.8.1 Phenomenological Models

Phenomenological BRDF models seek to emulate the characteristics of material reflection qualitatively. These models are ad hoc empirical formulas that attempt to reproduce the typical reflectance properties seen in real surface. There are numerous phenomenological models available in computer graphics and computer vision. Among them, few popular empirical BRDF models are presented here:

Phong model

Phong [27] introduced this empirical model in 1975 which dramatically improved the richness and realism of rendered image compared to the previous well-known Lambertian model. His model was designed to reproduce a glossy effect with minimal computation and provides simple parameters to control the appearance visually. The core idea is the empirical observation that for specular/glossy material, the reflection is strongest along the mirror direction R with respect to the light vector L, with a smooth falloff surrounding R. To describe this falloff, Phong [27] suggests using cosine between view vector, V and reflection vector R, raised to a certain power n.

The original formulation is:

$$K(L,V) = K_d + K_s . \frac{(V.R)^n}{N.L}$$

The original model is not physically plausible – it does not satisfy two main properties i.e. energy conservation or reciprocity that a BRDF model need to satisfy to be physically plausible [23].
A simple modification [23] that ensures these properties is as follows:

$$K(L,V) = \frac{K_d}{\pi} + K_s . \frac{n+2}{2\pi} . \frac{(V.R)^n}{N.L}$$

Though this model is simple and most well-known shading model in computer graphics, it is not supposed to simulate all real world material accurately since it has no Fresnel term and effective roughness term which exists in some of the model described in later sections.

Neumann et al. [25] showed that Phong model can not model the metallic surfaces efficiently. They proposed a modification of Phong model which they named as *stretch* Phong model for metallic surfaces:

$$K(L,V) = \frac{K_d}{\pi} + k_s . \frac{n+2}{2\pi} . \frac{(V.R)^n}{\max((N.L),(N.V))}$$

Blinn-Phong model

This model is a variant of the Phong model proposed by Blinn[3]. Blinn suggested to use Half-vector lobe i.e. cosine between Half vector, H and surface normal, N instead of cosine-lobe of original Phong model because it is cheaper to compute. Half-vector H is the half-way between L and V.

The formulation proposed by Blinn is:

$$K(L,V) = \frac{K_d}{\pi} + K_s . \frac{n+2}{2\pi} . (H.N)^n$$

This model is also the default shading model implemented in OpenGL. Ngan et. al.[22] showed that the half-vector based Blinn-Phong model perform better than Phong-model in almost all case of modeling the appearance.

Stretch Blinn model which a modification of Blinn-Phong by Neumann et al. [25] for metallic surfaces is as follows:

$$K(L,V) = \frac{K_d}{\pi} + k_s . \frac{n+2}{2\pi} . \frac{(H.N)^n}{\max((N.L),(N.V))}$$

Ward Model

Ward [40] proposed an empirical model in 1992 which is regarded as simple and efficient, but also designed to fit measured reflectance data to incorporate surface anisotropy. Ward claims that his model can fit measured reflectance data accurately.

He introduced an imaging Gonio-reflectometer to measure BRDF in his paper. Instead of the cosine lobe used by Phong, the Ward model is based on the elliptical Gaussian [23]. It has two

parameters, α and β, that define the spread of the lobe in the two direction. For isotropic materials, these two parameters are equal and the ward model has single parameter for isotropic materials.

The formula [19] is as follows:

$$K(L,V) = \frac{K_d}{\pi} + K_s . \frac{1}{\sqrt{(N.L)(N.V)}} . \frac{\exp[-\tan^2\theta_h (\frac{\cos^2\theta_h}{\alpha^2} + \frac{\cos^2\theta_h}{\beta^2})]}{4\pi\alpha\beta}$$

Where θ_h is the angle between surface normal, N and half-vector, H. However, recently Duer[6] shows that the model is not strongly energy-conserving. He proposes a modification to the model to make it strongly energy-conserving:

$$K(L,V) = \frac{K_d}{\pi} + K_s . \frac{1}{(N.L)(N.V)} . \frac{\exp[-\tan^2\theta_h (\frac{\cos^2\theta_h}{\alpha^2} + \frac{\cos^2\theta_h}{\beta^2})]}{4\pi\alpha\beta}$$

The isotropic version of *modified* Ward model, proposed by Neumann et al.[25] for metallic surface is as follows:

$$K(L,V) = \frac{K_d}{\pi} + K_s . \frac{1}{\max((N.L),(N.V))} . \frac{\exp[{}^{-\tan^2\theta_h}\!/_{\alpha^2}]}{4\pi\alpha^2}$$

Lafortune Model

In 1997, Lafortune et. al. [15] introduced a new approach to approximating the BRDFs of a material. They measured several materials' light reflection with a custom-built GonioReflectometer. The data was then fit, but instead of using traditional linear functions, they chose to use non-linear approximation with sum of one or more appropriate functions. Specifically, this model is a generalization of the cosine lobe model of Phong model with multiple steerable lobes. Their model also considered some important phenomena such as off-specular reflection, increasing reflectance and retro-reflection.

But, it has very unintuitive parameters which are hard to set values for. While this model is a non-linear basis for reflectance representation, it is commonly considered as a phenomenological BRDF model as well. The non-linear basis can be seen as a generalization cosine lobe:

$$K = B = [C_x l_x v_x + C_y l_y v_y + C_z l_z v_z]^n$$

Since its introduction, this model has become one of the most popular modes because of its generality and computational efficiency. However, Ngan et. al. [23] , who evaluated the performance of several popular BRDF models in terms of their ability to fit measured data of 100 types of materials, found that Lafortune model shows inferior performance most of the case compared to Cook-Torrance having same number of free parameters.

2.8.2 Physically-based BRDF Models

While phenomenological or empirical BRDF models seek to emulate the characteristics of material reflection qualitatively, physically-based model derive the quantities from first principles of physics. A number of well-known physically-based models, proposed by different researchers, will be listed here.

Cook-Torrance model

This popular physics-based model proposed by Cook and Torrance [5], derived from an early surface model called Torrance and Sparrow model [38], strives for as much physical realism as possible. In this model, the surface is thought to be made of planar microscopic perfect Lambertian reflectors called microfacets. Several of the terms in the lighting equation deal with how these microfacets are oriented, masked and shadowed. It uses a physically-based function for its specular component and also includes explicit Fresnel term. Having this term, this model can simulate the increasing specularity near grazing angle. That is why this model can give photorealistic image and realistic look of metallic material. According to their formulation, the reflectance at a particular light/view combination is a function of the number of aligned microfacets, the amount of shadowing and masking between microfacets, and the reflectance of ideal mirror.

The formula is as follows:

$$K(L,V) = \frac{K_d}{\pi} + \frac{K_s}{\pi} \cdot \frac{DGF}{(N.L)(N.V)}$$

Where,

$$G = \min\{1, \frac{2(N.H)(N.V)}{(V.H)}, \frac{2(N.H)(N.L)}{(V.H)}\}$$

$$D = \frac{1}{m^2 \cos^4 \theta_h} . \exp[-(\frac{\tan \theta_h}{m})^2]$$

G is the geometric attenuation term which approximates the shadowing and masking effects, while D is the distribution of the microfacets. F is the Fresnel term which governs the reflection for smooth mirror. Ngan et. al. [23] , who evaluated the performance of several popular BRDF models in terms of their ability to fit measured data of 100 types of materials, found that Cook-Torrance model perform the best in most cases.

Ashikhmin model

Ashikhmin et al. [1] proposes a model which is also based on microfacet distribution like Cook-Torrance. While the shape of microfacet distribution in Cook-Torrance and its variant He-Torrance-Sillion-Greenberg model [12] is assumed to be Gaussian [23], Ashikhmin proposes this model based on arbitrary distribution of microfacets.

The expression for the Ashikmin et al. model is as follows:

$$K(L,V) = \frac{K_d}{\pi} + \frac{n+1}{8\pi} \cdot \frac{(N.H)^n F}{(V.H)\max[(N.L),(N.V)]}$$

Oren-Nayar model

Oren and Nayar [26] created this BRDF model in the hope to 'generalize' the Lambertian diffuse lighting model, since the Lambertian model is not suitable for representing certain rough surfaces like a cylindrical clay base, whereas in this case their model is much better. This model can reproduce several rough surfaces very well, including wall plaster, sand, sand paper, clay, unglazed ceramics and others.

Similar to Cook-Torrance, it is also based on a collection of microfacets, but these microfacets are modeled as perfectly diffuse surface. However, due to complex shadowing effects, the overall BRDF is not lambertian. It is however very computationally expensive. The readers are referred to their paper for full formulation.

HTSG model

This model, an extension of Cook-Torrance model, created by He-Torrance-Sillion-Greenberg [12] is regarded as the most complex and also comprehensive analytical BRDF model. In this model, they assumed reflection from arbitrary surface can be divided into first surface reflection and multiple surfaces and/or subsurface reflection. This model can be employed for ray tracing or extended radiosity method. It can also be applied to metallic, non-metallic & plastic material. HTSG model, having effective roughness term, can simulate some surfaces very well, like white paper that shows reflectance which varies dramatically near grazing angles due partly to the decrease in effective roughness. Unlike most other models, this model takes polarization and other wave phenomena into account. The readers are referred to their paper for full formulation.

2.9 BRDF Measurement and Parameterization

Apart from using analytical BRDF models as described in previous section to approximate surface reflectance, there is a traditional device called gonio-reflectometer for measuring BRDFs of a surface. Though analytical models are very simple and easy to use, they usually approximate the reflectance of a surface and can not model complex surfaces accurately. On the other hand, direct measurement by gonio-reflectometer gives accurate BRDF but the acquisition system is usually very complex. This section describes BRDF measurement system, calibration system and data processing steps.

2.9.1 Measurement System

Traditionally, BRDFs of a surface are measured using gonio-reflectometers which consist of a light source and a detector. Researchers have been proposing more and more efficient gonio-reflectometers for the last few years. Among them, image-based measurement system, proposed by Marschner [19], is widely used till now.

Matusik [21] and Ngan [22] also used the same setup proposed by Marchner and extended the setup for measuring anisotropic BRDF. Inspired by the Marchner and Matusik's work, we have built up our image-based measurement system for measuring isotropic BRDF.

Image-based BRDF Measurement System

Image-based acquisition system is a BRDF measurement process which can measure surface reflectance rapidly, completely and accurately. The main parts of this system are a digital camera as a detector, a light source, a precise computer-controlled turntable and a homogeneous sphere sample of target material. The light source is mounted on an arm to the turntable which facilitates the lamp to orbit the measurement sample placed at the centre of rotation; the camera and the sample are stationary. Our image-based system is shown in figure 2.6. The fixed camera takes the images of the sample under varying illumination from an orbiting light. In an image of a curved object taken using the detector, every pixel is in effect a BRDF measurement. We use a 5 watt *LED* as a light source and *Cannon Mark-II* as a detector.

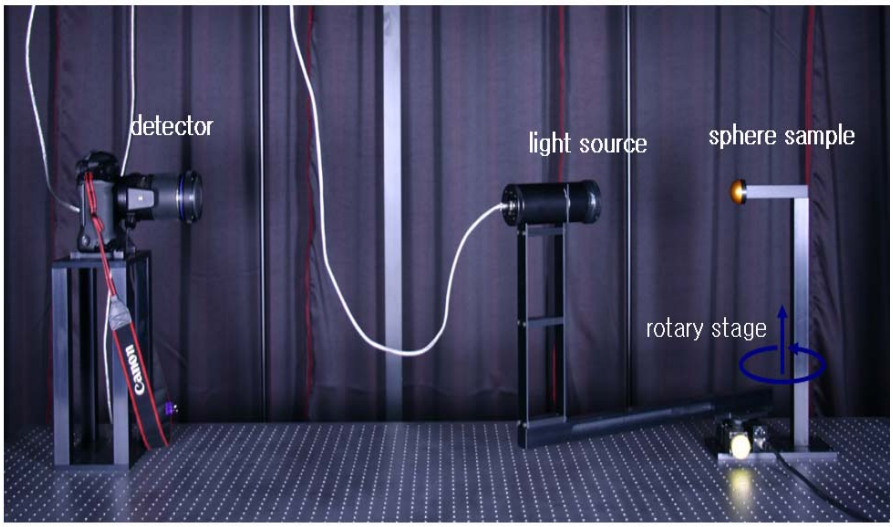

Figure 2.6: Image-based BRDF measurement system

Acquisition Process

The basic process is presented here: the light source moves in increment of 1 degree from the point exactly in front of the camera to the position exactly opposite the camera. For each position of the light, we take 10 images with different exposure time and combine them to

generate one high dynamic range image, which records the BRDF data for this light position, and in which each pixel on the sphere is a separate BRDF measurement.

Geometric and Radiometric calibration

To turn the camera image into accurate BRDF measurement, it requires both geometric and radiometric calibration. Geometric calibration establishes the relative positions of the light source, sample and camera for each measurement image, and radiometric calibration determines the irradiance from the source and the relationship between pixels values and radiance reflected from the sample.

In geometric calibration, we recover the intrinsic parameters of the camera using camera calibration method of Robertson et al. [31]. We also measure the radius of painted sphere and calculate the centre of sphere with the known parameters. Then we set up the geometric relationship of camera, light source, and hemisphere. For radiometric calibration, we recover the response curve of the camera which describes the relationship between pixel values and luminance (irradiance).

2.9.2 BRDF Parameterization

The measured BRDF samples have to be stored in a compact table using specified parameterization approach. There are a number of parameterization methods for storing BRDF data, among them standard parameterization and Rusinkiewicz parameterization are widely used. A brief description of them is presented here:

Standard Parameterization

This is the most commonly used parameterization based on spherical coordinate. Each direction, incident and outgoing, is represented by spherical angle: azimuth and elevation angle. In the standard surface frame, the normal ***n*** lies on the z-axis, the surface tangent vector, ***t*** lies on the x-axis and the surface binormal, ***b*** which can be obtained by the cross-product of ***t*** and ***n*** lies on the y axis. The elevation angle theta of both incident vector and outgoing vector is measured relative to ***n*** and azimuth angle relative to ***t***, as shown in figure 2.7.

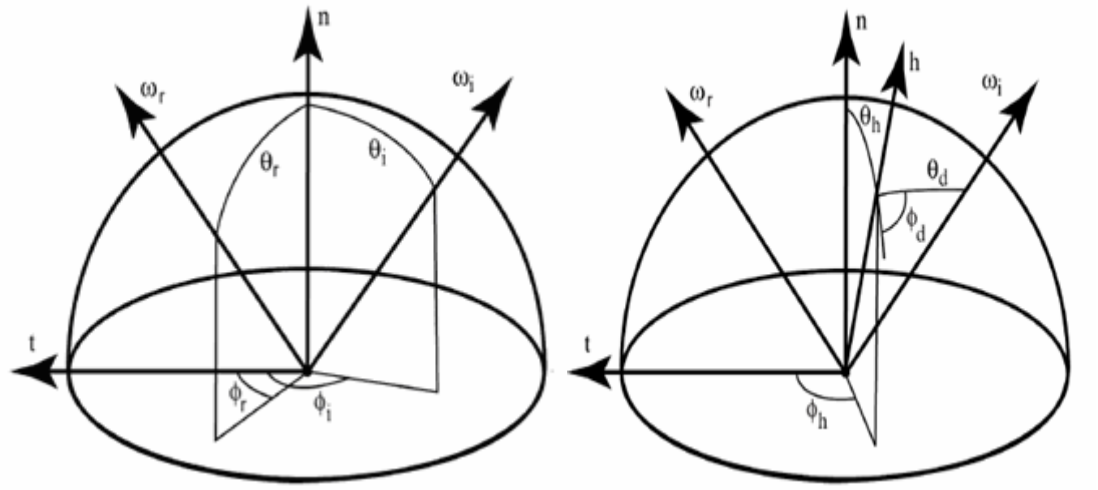

Figure 2.7: Standard (left) and Rusinkiewicz parameterization (right) (image from [33)

Rusinkiewicz Parameterization

Rusinkiewicz [33] suggests an alternative BRDF parameterization which is based on half-angle vector, ***h*** and a difference vector, ***d*** instead of incident and outgoing vector. The purpose of this parameterization is to align prominent features of the BRDF, such as specular peak, with coordinate axes. For instance, the power of the specular reflection is not directly dependent on the position of the incoming or outgoing vectors. The specular power is, however, usually directly dependent on the position of the half-angle vector. Using Rusinkiewicz parameterization, it is often possible to separate the specular reflection from diffuse reflection more easily than in a standard parameterization. This parameterization allows sampling specular peak more densely than off-specular peak which facilitate to model some specular materials' appearance. The two vectors ***h*** and ***d*** can be determined as follows:

$$\vec{h} = sph(\theta_h, \phi_h) = \frac{\vec{w}_i + \vec{w}_o}{\left\| \vec{w}_i + \vec{w}_o \right\|}$$

$$\vec{d} = sph(\theta_d, \phi_d) = rot_{\vec{b}, -\theta_h} rot_{\vec{n}, -\phi_h} \vec{w}_i$$

2.10 The Rendering Equation

Given a scene description consisting of the geometry, the reflection properties and a specification of the light source one can render the scene solving rendering equation formulated by Kajiya [14]:

$$L_0(\vec{x}, \hat{v}^g) = L_e(\vec{x}, \hat{v}^g) + \int_{\Omega+} f_r(\vec{x}, \hat{l}, \hat{v}).L_i(\vec{x}, \hat{l}^g)(\hat{n}.\hat{l}^g)d\hat{l}$$

It is the integral equation for the incident illumination at one point from the upper hemisphere $\Omega+$, with the following definitions for the other quantities: $L_e(\vec{x}, \hat{v}^g)$ is the radiance emitted from the surface at point $\vec{x}$ into the global viewing direction $\hat{v}^g$ and is only relevant for light sources; $f_r(\vec{x}, \hat{l}, \hat{v})$ stands for BRDF at point $\vec{x}$, that is the fraction of radiance incident from direction, $\hat{l}$ that will be reflected in the outgoing direction, $\hat{v}$; $L_i(\vec{x}, \hat{l}^g)$ denotes radiance incident at surface point $\vec{x}$ from global light direction $\hat{l}$ and $\hat{n}$ is the normal.

Dropping the emitting term and reformulating for isotropic BRDF coordinate system, the rendering equation can also be expressed as:

$$L_r(\theta_r, \phi_r) = \int_{\Omega+} f_r(\theta_i, \theta_r, \phi_{diff}).L_i(\theta_i, \phi_i) \cos\theta_i d\omega_i$$

A number of algorithms have been proposed to solve the first equation especially for global illumination. They can be grouped into two main categories: Finite element methods and Monte Carlo algorithms. Finite elements methods subdivide the surface in the scene into patches or elements and simulate the energy transport between sending and receiving patches. Radiosity and hierarchical radiosity methods are representatives of finite element method. Another class is so Monte Carlo algorithms where basically a large number of rays are traced through the scene.

In this thesis, we use two simplistic approaches to render scene: local illumination using point light source and environment mapping technique. We present these two techniques in following sections:

Local Illumination

If we use only point light source, the evaluation of rendering is simplified. In this case the local illumination is evaluated as:

$$L_0(\vec{x}, \hat{v}^g) = \sum_{j=0}^{n} f_r(\vec{x}, \hat{l}_j, \hat{v}).\frac{I_j}{r_j^2}.(\hat{n}.\hat{l}_j^g)$$

Here, I_j is the j-th point light source and r_j^2 is the squared distance from **x** to the light source.

Environment Maps

A simplistic approach to render an object is an environment map representing fixed incident illumination $L_{env}(\hat{l}^g)$. The environment is assumed to be at infinity and there is no light emitted or reflected by the object into the environment. The equation is:

$$L_0(\vec{x}, \hat{v}^g) = \int_{\Omega+} f_r(\vec{x}, \hat{l}, \hat{v}).L_{env}(\vec{x}, \hat{l}^g)(\hat{n}.\hat{l}^g)d\hat{l}$$

Environment maps without shadowing can be successfully applied in hardware-accelerated algorithms.

Chapter 3

Coating/Paint Microstructure

Coatings are becoming increasingly important in automotive, currency and cosmetic applications because of their ability to give a product appealing look which eventually creates widespread consumer appeal. However, there are different types of coatings with various composition of microstructure which includes pigments, flakes, transparent clearcoat and others. The composition of coating microstructure plays the major role in determining the final appearance of coating. This chapter focuses on the different types of paint and paint microstructure. In the following sections, we start by the treatment that applied before painting a surface called surface treatment. We then explain composition of paint or coating, followed by different types of paint. Finally, we describe the effect of the major components of coating microstructure on the final appearance of coated surfaces.

3.1 Surface Treatment before Painting

Traditionally, there are three surface treatments provided on the surface before painting the sheet of metal. The first treatment acts against corrosion. Then a gray layer called electrocoat is applied on the sheet of metal to suppress surface large amplitude deformations. Finally, another gray layer is applied to level the surface and protect it from loose chipping. This layer is called Primer layer. Electrocoat and primer layer are separately baked. After applying these surface treatments, the actual paint or coating is applied to the surfaces.

3.2 Composition of Paint

The paint may consist of several layers for special purposes, but the two-layer paint is most widely used. In this thesis, we restrict our consideration to two-layered paints that are composed of clearcoat and basecoat layer. Basecoat and clearcoat are baked together without an intermediate firing. We in this section review the structure of each of the layer with their special properties. The composition of paint microstructure is shown in figure 3.1.

Clearcoat or Overcoat

For all the coatings, the front surface is a clear and smooth transparent varnish called clearcoat or overcoat. The thickness of this layer is usually 35-45 µm. The clearcoat is a protective layer against weathering. It also carries on the surface leveling and gives gloss property of the surface.

Basecoat

The second layer called basecoat is composed of a number of components namely flakes, binders, solvents, additives and so on. The thickness of basecoat normally varies between 15 to18 µm. Binders are generally resins, more or less transparent bodies. They bind paint components together. The role of additives is to give special properties to the coating such as resistance, hiding powder, pigment dispersal.

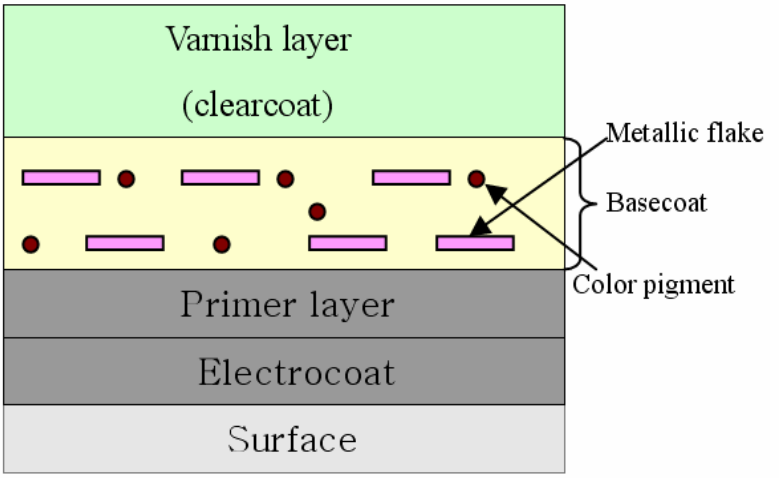

Figure 3.1: Composition of Coating microstructure (image adapted from [7])

One of the most important components of basecoat is flake which is responsible for creating sparkles, a prominent feature of paint. Flakes are generally very thin platelet which can be readily oriented into parallel layers due to their shape. Flakes can treated as tiny colored mirrors. Flakes are characterized by the following factors: the fraction of paint area they occupy, variation of their orientation, their thickness, the optical properties of their body and coating, and also some other parameters.

Basecoat is the most important layer between the two layers of a paint and solely responsible for the appealing appearance of the metal surface on what they applied. Since it is composed of various components, different composition of basecoat makes different paint.

3.3 Types of Paint or Coating

While the front surface layer, clearcoat, is almost same for all paints, the basecoat may vary for different purposes since it has many components. Different composition of basecoat's components may form different paints and their appearance also varies according to their composition. There are mainly three types of paint or coating which has different composition of basecoat: solid or conventional paint, metallic paint and pearlescent paint.

Solid or Conventional paint

This is the most simple and conventional paint that has no special lighting effect. The basecoat of these types of paint only contains solid paint film. It does not have any flakes. That is why it can not provide any sparkles and they provide very simple appearance. The reflectance of these types of paint is assumed to the same for all direction. The composition of basecoat of these types of paints is shown in figure 3.2a.

Metallic paint

Metallic paint is one of the most widely coating in different applications because of its ability to give a product appealing look. The basecoat of metallic paint contains flakes, color pigments, binders and others. The flakes of metallic paint basecoat are single layered colored platelets which are often made by aluminum. Their size varies from 5 to 45 micron and thickness varies from 0.1 to 1 micron.

Aluminum flakes act like small mirrors that reflect the incident light in specular direction. Paint appearance changes with the observation and lighting conditions. At different visual angles, the observer can see either the aluminum flakes or the colored film. The basecoat composition of metallic paint is shown in figure 3.2b.

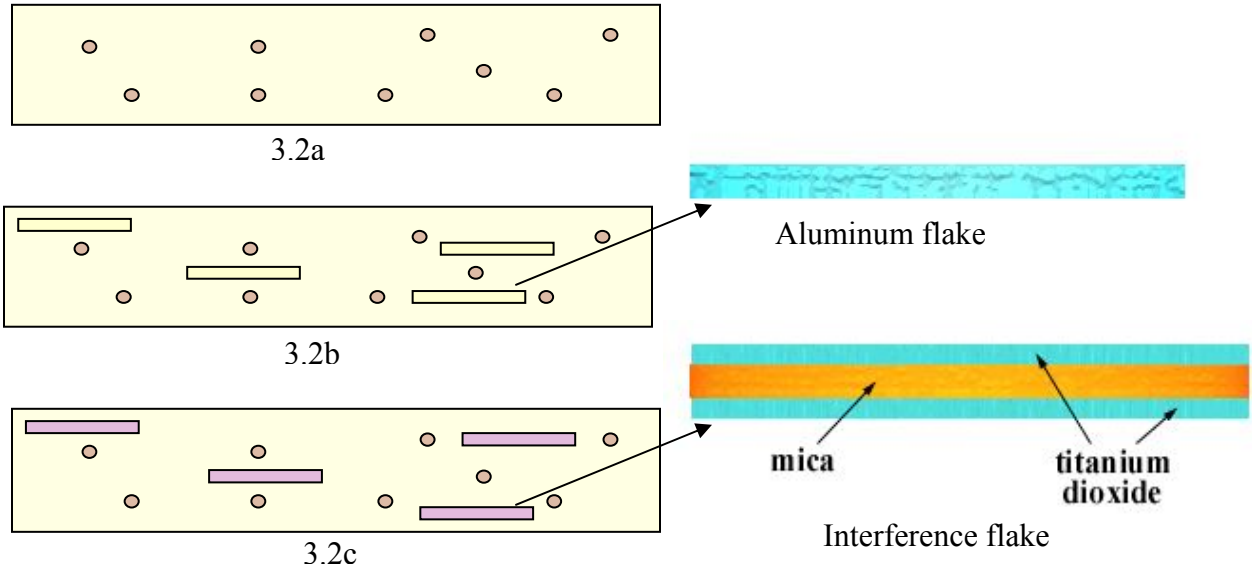

Figure 3.2: Basecoat of different types of paints. (3.2a) conventional (3.2b) metallic and (3.2c) pearlescent paint.

Pearlescent paint

This paint is another widely used coating in automotive industry, nowadays. The main difference between the metallic and pearlescent paint is their flakes' structures. While metallic flakes are considered as single-layer colored platelets, the pearlescent flakes consist of two layer of coating, which makes paint appearance more intricate. The two layer flakes is usually of a material with low refractive index, such as mica, coated with highly refractive metal oxide, such as titanium dioxide or iron oxide.

The most widely used pearlescent pigments or flakes are mica platelets coated with precise layer of iron oxide or titanium dioxide. The flake of pearlescent paint also called interference flake. Pearlescent flakes manipulate light through interference, creating iridescent shifts of color similar to those seen with oil slicks, soap bubbles and peacock feathers. When the incident light reaches the flakes, there is a combination of absorption, reflection and interference phenomenon. The reflected color is controlled by the nature of the metallic oxide, the thickness of the oxide layer and the size of the mica pigment.

3.4 Appearance attributes of Coated Surfaces

The appearance of a coated surface depends on the complex light interaction properties with the components of its microstructure. Hence, the composition of its microstructure affects the appearance of coated surfaces. Though any of the microstructure components can influence the appearance, we in this thesis only consider the effect of flake on the appearance of coated surfaces since the effect of flake is greater than others. We also disregard the difference in flake structure between metallic and pearlescent flakes.

Presence of flakes

While solid or conventional coating does not have any flake, metallic and pearlescent paint possess it. The effect of presence of flakes is shown in figure 3.3. While coating with no flakes gives satin appearance, coating with flakes gives a more appealing or sparkling look.

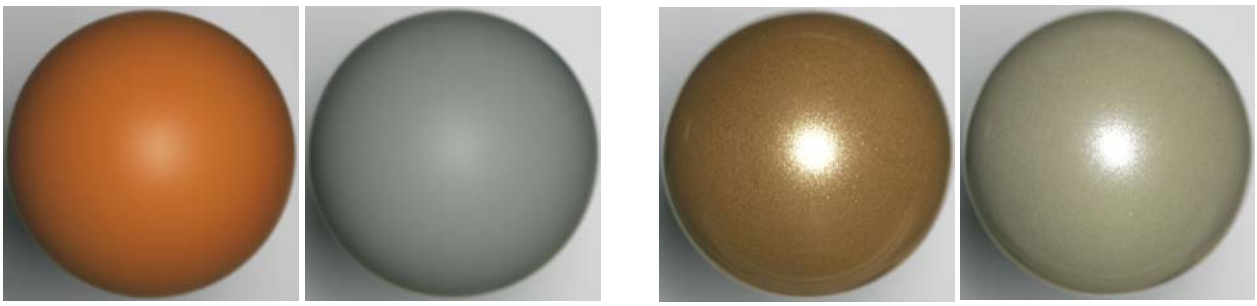

Figure 3.3: Effect of presence of flakes on the appearance of coated surfaces. First two figure show gold and silver coated surfaces respectively with no flakes (a type of solid or conventional coating). Third and fourth figures are same coating but with 2% flake in their microstructure with average flake size approximately 25 microns.

Density of flakes

The variation in density of flakes of a coating microstructure affects the appearance as shown in figure 3.4. From this figure, it can be seen how a slight flake density variation changes the appearance of coated surfaces. It is distinct that density of sparkles is determined by density of flakes.

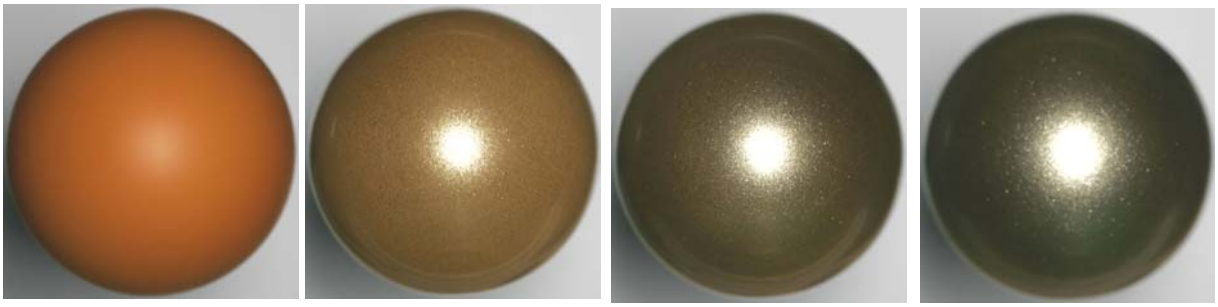

Figure 3.4: Effect of flake density variation on the appearance of a gold coated surface. From left: gold coated surface with flake density 0%, 2%, 5%, 8% respectively in their microstructure. All the samples have same average flake size of approx. 25 micron.

Average Size of Flakes

The average size flakes determine the average size of sparkles, hence influences the appearance of coated surface which is shown in figure 3.5. As we can see from the figure, there is subtle difference in the appearances of these samples for the slight variation in their microstructural flake size.

Figure 3.5: Effect of flake size variation on the appearance of a gold coated surface. From left: coated surface with average flake size 15, 20, 25 micron respectively in their microstructure. All the samples have same flake density of 8%.

Chapter 4

Microstructure-based Modeling

This chapter describes the overall approach of microstructure-based modeling of coated surfaces. We first introduce notable prior works by different researchers on coating or paint appearance simulation. Then, we describe our full process of modeling approach starting from an overview of the dataset we use to rendering.

4.1 Prior Work

Various researchers have been trying to simulate the appearance of paint, especially metallic paint, in different ways. Ershov et al. [8] proposed a paint-composition model for modeling pearlescent appearance. In their approach, they decomposed paint layer into stacks of imaginary thin sub layers and then these layers is assembled by a recursive assembling procedure to get the final appearance. Dumont-Becle et al. [7] used a multi-texturing approach for paint appearance simulation. In multi-texturing approach, each appearance criterion of the coating such as layers is represented by different types of textures and final appearance is obtained by combining all the textures. Figure 4.1 shows the multi-texturing process of Dumont-Becle et al. [7]. Recently, Guenther et al. [11] simulated the car paint appearance realistically. At first, they acquired real reflectance data with image-based measurement system, as described in chapter 3. They then fitted multi-lobe Cook-Torrance [5] model to the measured data using non-linear optimization technique to get the parameters. They sampled their measured data using Rusinkiewicz parameterization [33] technique (described in chapter three). Finally, they used a real-time ray tracing technique, proposed by Ingo Wald [39], for realistic rendering of car paint with fitted Cook-Torrance parameters.

It should be noted that most of the above mentioned prior research works did not take account of coating microstructure. Either they completely ignored the effect paints' microstructure at the time of rendering or they did not vary the components of their microstructure to see the difference in appearance that they entail (presented in chapter 3). This thesis tries to fill this gap.

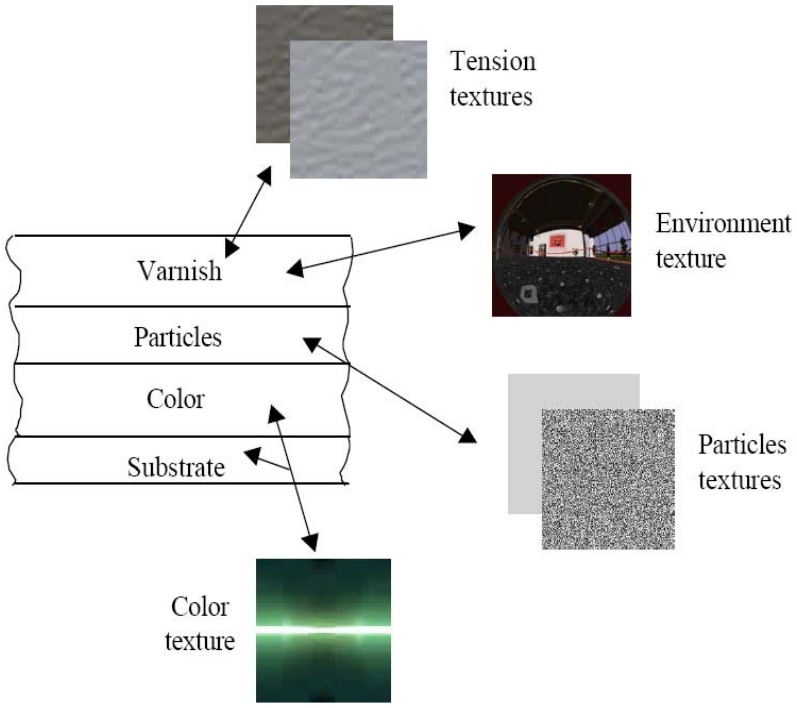

Figure 4.1: Multi-texturing approach of Dumont-Becle et al. [7]. Each appearance attributes is represented by different types of texture.

4.2 Data Set

We use two sets of measured BRDF database. The first one is of Matusik et al. [20] which is available on web. A comprehensive description of their data can be found in [20].Though the BRDF database of Matusik et al. has a data set of 100 BRDFs which includes a number of samples including metals, plastic and painted surface and fabrics, we only use data of painted surfaces since our work is on painted or coated surfaces. It should be noted that we do not know about the composition of microstructure of Matusik et al. [20] paint sample. Nonetheless, we use their well known data for experimental purposes.

The second set of database we use is our own measured data. We use hemisphere-shape samples of paint for measuring the BRDFs using our image-based acquisition system proposed by Marchener et al. [19]. A brief description of our image-based system is presented in chapter 3. Each hemisphere sample we use is covered with uniformly distributed coating varying in their microstructural composition by professional painting studio.

We have collected a wide range of coated samples with different composition of microstructure, as shown in figure 4.2. Among the various microstructural components of a coating microstructure, the flake plays major role on its appearance (see chapter 3 for the flake effect on the coating appearance). Therefore, for this thesis, we select 16 samples among the wide range of coated samples with varying flake density and size, as shown in figure 4.3a and 4.3b. Figure 4.3a shows the selected samples for gold coating and figure 4.3b is for silver coating. The first two rows of the figures show samples differing in flake density with same flake size and third row shows samples possess same flake density with flake size variation.

Figure 4.2: Coated samples differing in their microstructural composition

4.3 Data Processing

After acquiring BRDFs of a coated hemisphere sample by our image-based acquisition system described in chapter 3, these data should be processed accurately for fitting. The first database of Matusik et al. what we use was originally represented using Rusinkiewicz parameterization [] based on half-vector and tabulated non-uniformly to optimize for rendering quality. Recently, this parameterization has been changed to standard parameterization.

For our own measured data, we record the measured BRDF samples in a compact BRDF table using standard parameterization. We group all the valid BRDF samples into bins uniformly spaced in the 3D domain of an isotropic BRDF defined by θ_{in}, θ_{out} and Φ_{diff}. We discretize θ_{in}

and θout into 90 bins and Φ_{diff} into 180 bins. Readers are referred to chapter three for a description of standard and Rusinkiewicz parameterization.

Each tabulated BRDF in the case of regular sampling of 1 degree contain 90x90x180x3 = 4,37,4000 which is a large amount of values. Aside from this amount being impossibly large to manage, using this number of samples would slow the fitting down to a significantly degree that it is practically impossible to perform. Any kind of reduction in the number of samples required to perform a fitting would be therefore be useful. We therefore manually select 3000 to 4000 BRDFs for each coated sample for fitting purposes by ensuring no significant information has been lost.

4.4 Fitting BRDF model to measured data

A core part of our modeling technique is to fit analytical BRDF models to real measured data. Data fitting requires two things: a data fitting algorithm and the model to fit. The data fitting algorithm which we use is presented in section 4.4.2. We have presented a wide range of existing reflection model in chapter three. Among them, we have selected three BRDF models described in section 4.4.1. Most of the techniques presented in this section are adapted from [23].

4.4.1 BRDF models for fitting

We have presented various existing BRDF models developed by different researchers in chapter three. Among them we have selected few BRDF models to fit to measured data based on the result of Ngan et al.[22] who evaluated the performance of several popular BRDF models in terms of their ability to fit the measured data of 100 types of materials which includes plastic, fabric, paint etc. Ngan et al. [22] found that Ashikhmin and Cook-Torrance model performs the best in most cases. They also concluded that, between Phong and its variant Blinn-Phong model, half-vector based Blinn-phong model performs better than reflection-vector based Phong model. Based on these facts, we adopt their two best-performed physically-based models, Cook-Torrance and Ashikhmin et al. model and one empirical model Blinn-Phong for our analysis. We also briefly made experiment Neumann's modification of Cook-Torrance and Blinn-Phong which is called *stretch* Blinn-Phong and *stretch* Cook-Torrance BRDF models for metallic surfaces. We do not consider Oren-Nayar and Lafortune model because these models are intended for the

rough surfaces while painted surface is not rough. Readers are referred to the chapter 3 for the description of each BRDF model.

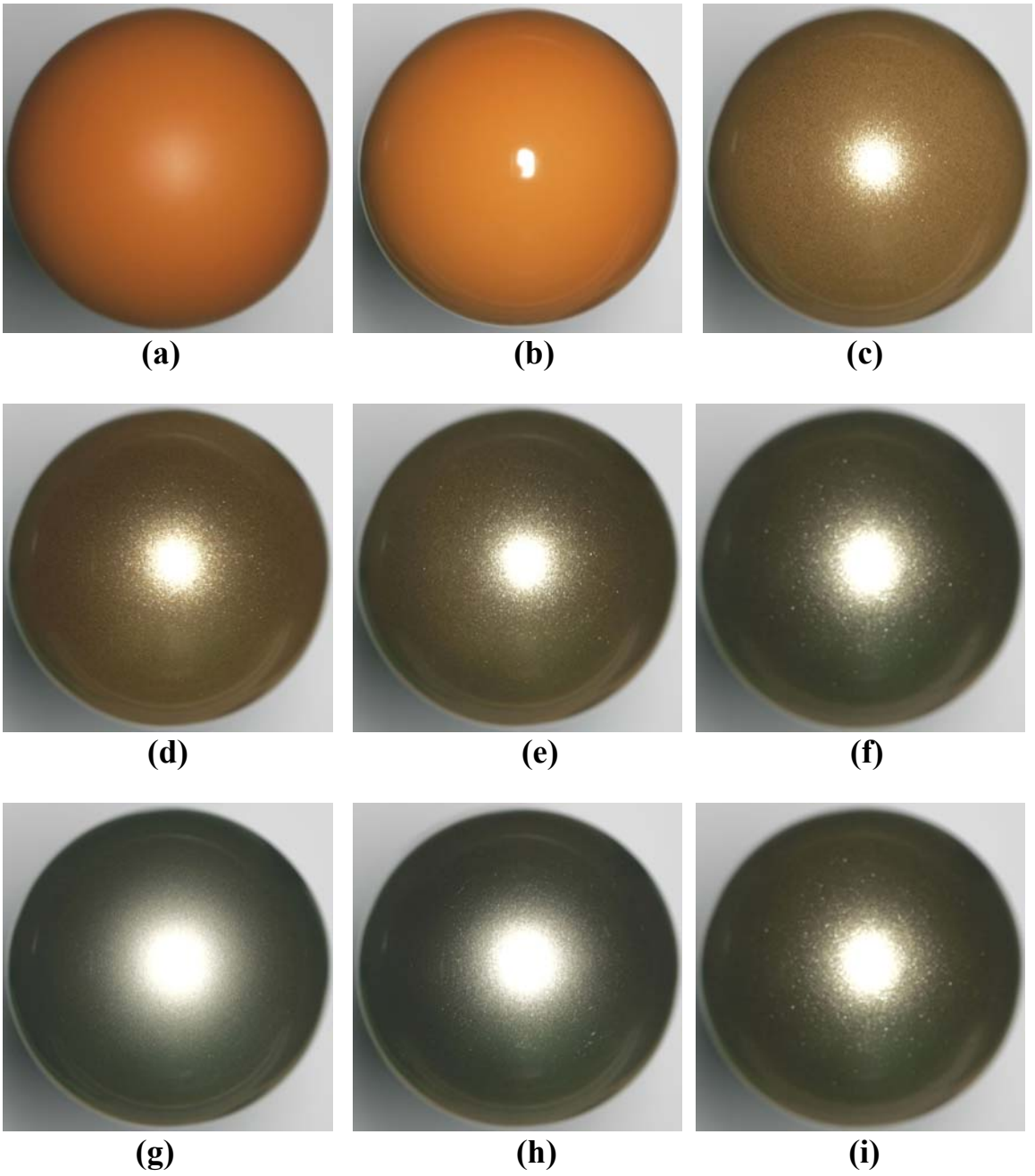

Figure 4.3a: Gold coated hemisphere samples differing in their composition of microstructure. First two rows show samples differing in their flake density but of same flake size and third row shows samples with same flake density but of varying flake size. Samples (a) to (f) have same average flake size of 25 micron but 0%, 0%, 2%, 3%, 5% and 8% flake density respectively. Samples (g) to (i) have same flake density of 8% but differing in their average flake sizes with 15, 20, 25 micron respectively.

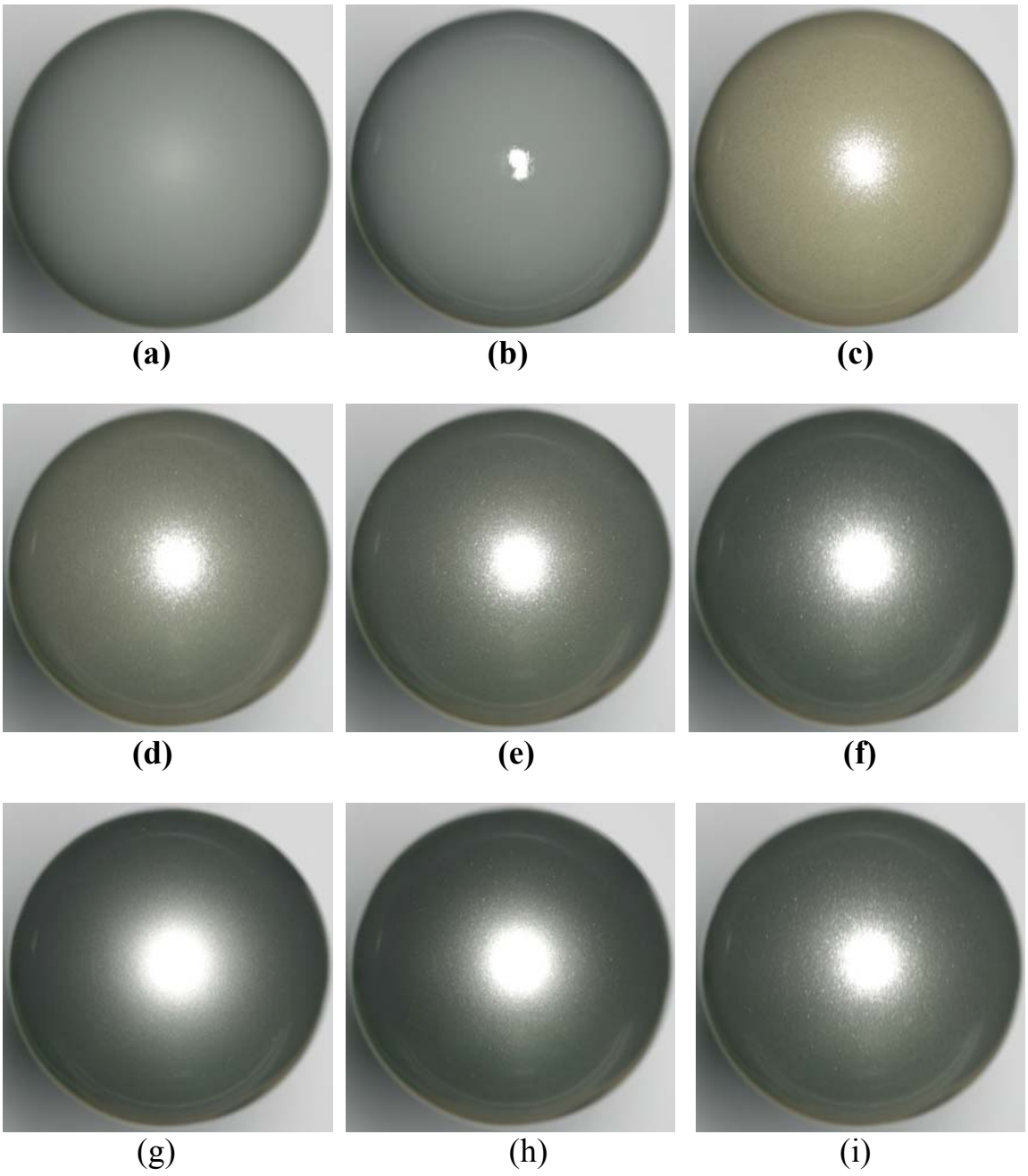

Figure 4.3b: Silver coated hemisphere samples differing in their composition of microstructure. First two rows show samples differing in their flake density but of same flake size and third row shows samples with same flake density but of varying flake size. Samples (a) to (f) have same flake size of 25 micron but 0%, 0%, 2%, 3%, 5% and 8% flake density respectively. Samples (g) to (i) have same flake density of 8% but differing in their flake sizes with 15, 20, 25 micron respectively.

To evaluate the performance of the analytical models, we enforce the diffuse contribution of the all models to be lambertian or ideal diffuse. Hence, for each color channel, all BRDF models can be expressed with two parameters, k_d and k_s, for diffuse and specular color and a variable number of parameters p_0, p_1, p_2,etc for specular lobe:

$$M = k_d + k_s * (p_0, p_1, p_2 ...)$$

Table 4.1 shows the required parameters of each of the BRDF models which need to be determined from fitting for each of three color channels R, G and B. Readers are referred to chapter 2 for the equation of models and each parameter name.

BRDF Models	**Features**	**Parameters** (to be determined)
Blinn-Phong	Phenomenological	k_d, k_s, p_0
Cook-Torrance	Physically-based	k_d, k_s, p_0, p_1
Ashikhmin	Physically-based	k_d, k_s, p_0, p_1
Stretch Blinn-Phong	Phenomenological	k_d, k_s, p_0
Stretch Cook-Torrance	Physically-based	k_d, k_s, p_0, p_1

Table 4.1: The parameters BRDF models to be determined from fitting

4.4.2 Fitting Algorithm

Since the BRDF models presented above are nonlinear expressions, the fitting process requires non-liner optimization. We apply a constrained nonlinear optimization technique based on a sequential quadratic programming (SQP) technique. We use a standard nonlinear Levenberg-Marquardt [14] [25] algorithm for that purpose. The goal of the optimization is to minimize the error metric *E(p)* which is defined as the root mean squared error between the measured BRDF, M and the BRDF of the target model, K weighted by the cosine of exitant angle, θ_v given parameter vector, **p** :

$$\text{min}imize,\ E(p) = \sqrt{\sum\ [M(\omega_i, \omega_o)\cos\theta_v - K(\omega_i, \omega_o; p)\cos\theta_v]^2}$$

Like any other nonlinear optimization, the quality of the fit is dependent on a good initial guess of the parameters to be determined. To ensure that the optimization converges to the global minimum, we visually inspect the fitting quality of the result and when necessary, restart the optimization from a different set of initial guesses.

In constrained optimization, the general aim is to transform the main problem into an easier sub problem that can then be solved and used as the basis of an iterative process. Quadratic programming concerns the minimization or maximization of a quadratic objective function that is linearly constrained. In SQP, a QP sub problem is solved for each major iteration. SQP methods represent the state of art in nonlinear programming methods.

4.4.3 Qualitative Comparison of Results

The result of the optimization process described above is the fitted parameters and visual representation of the fitting. However, a visual representation of the data fitting results visualizes a select part of the dataset, but does not give enough information. In order to judge the results appropriately and to determine the difference between the different fittings it is necessary to make a qualitative comparison of the resulting fitting to each other.

In order to determine a meaningful measure we need to compare the fitting results of different BRDF models. A common method of comparison is to use the Signal to Noise ratio (SNR) as a comparison. The Signal to Noise ratio (SNR) is an estimation of the ratio of important data (signal) to unimportant or deviant data (noise). Consequently, the higher the SNR value is the better the model fit [13].

There are various different metrics to calculate the SNR. The one which is commonly applied in graphics and computer vision to compare images is calculated as follows:

$$mean\ \ squared\ \ error\ , MSE\ = \frac{1}{N}\sum_{i}^{N}(m_i - s_i)^2$$

$$Variance\ \ , VAR\ = \frac{1}{N}\sum_{i}^{N}(m_i - \overline{m})^2$$

$$SNR\ = 10\ \log_{10}(\frac{VAR}{MSE})$$

Here, s_i is the BRDF model predicted value; m_i is the measured value, *m-bar* is the mean of the measured values in the dataset and *N* is the number of samples in the set. We performed a comparison of the results using the SNR as a measure of accuracy.

Chapter 5

Results and Discussions

In this chapter, we will present and discuss results of the microstructure-based modeling of coated surfaces that described in chapter 4. We first present the fitting results with their parameters in section 5.1. Then we provide rendering result based on the fitted parameters as well as real measured data in section 5.2. Finally, we conclude this chapter in section 5.3.

5.1 Fitting Result

We fitted five carefully selected existing BRDF models to the measured BRDFs of coated hemisphere-shape samples using nonlinear optimization technique to determine the appropriate parameters of the BRDF models for those samples. We have described our BRDF models selection process, coated hemisphere-shape samples and optimization technique in chapter 4. A sample visualization of Cook-Torrance BRDF model's fitting result for incidence plane specular BRDF data of a gold coated hemisphere-shape samples having 8% flake density in their microstructure for red, green and blue channels is shown in figure 5.1a, 5.1b and 5.1c respectively. The *diamond-shaped* symbol in figure 5.1a, 5.1b and 5.1c denotes the measured BRDF value and *star-shaped* symbol denotes the Cook-Torrance's fitted value. The fitted Cook-Torrance parameters with goodness of fit i.e. Signal-to-Noise (SNR) ratio of Cook-Torrance model for figure 5.1a, 5.1b and 5.1c is provided in table 5.1. Readers are referred to chapter 2 for a description of Cook-Torrance model and the parameters' name shown in table 5.1.

After fitting the BRDF models to the measured data of all coated samples which have varying composition of their microstructure, we perform a comparison of BRDF models BRDF models in terms of their ability to approximate the reflectance of coated samples and hence, determine the best existing model for coating material. Sample figures of BRDF models fitting comparison are shown in figure 5.2. The X-axis denotes the variation of microstructural components (for figure 5.2, flake density variation) and Y-axis shows the goodness of fit or SNR ratio. It should be noted that the higher the SNR value, the better the fitting capability of the model.

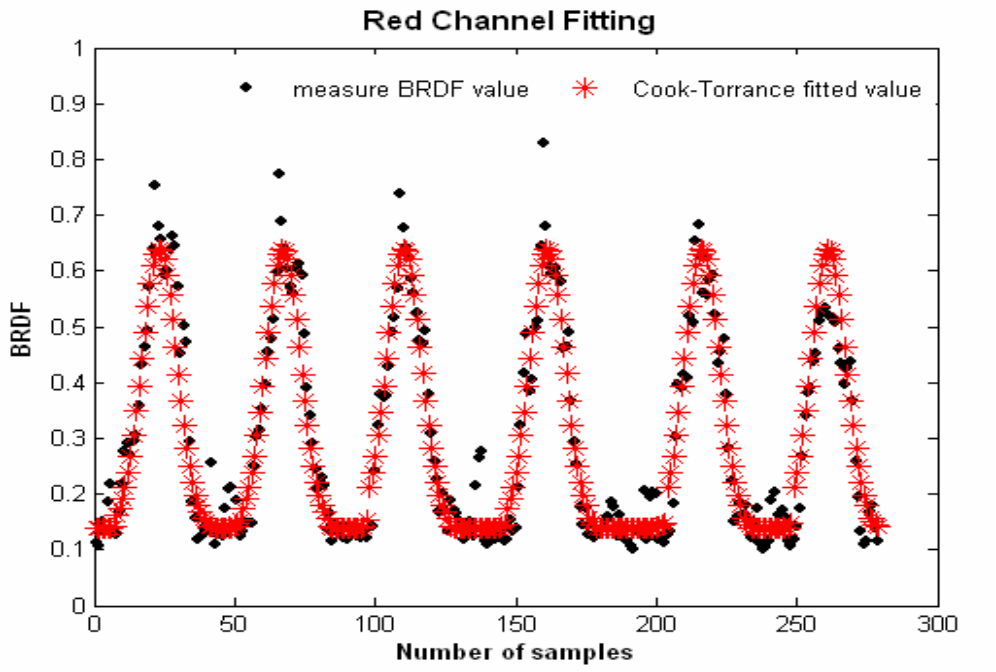

Figure 5.1a: Sample red channel fitting result for a gold coated hemisphere sample.

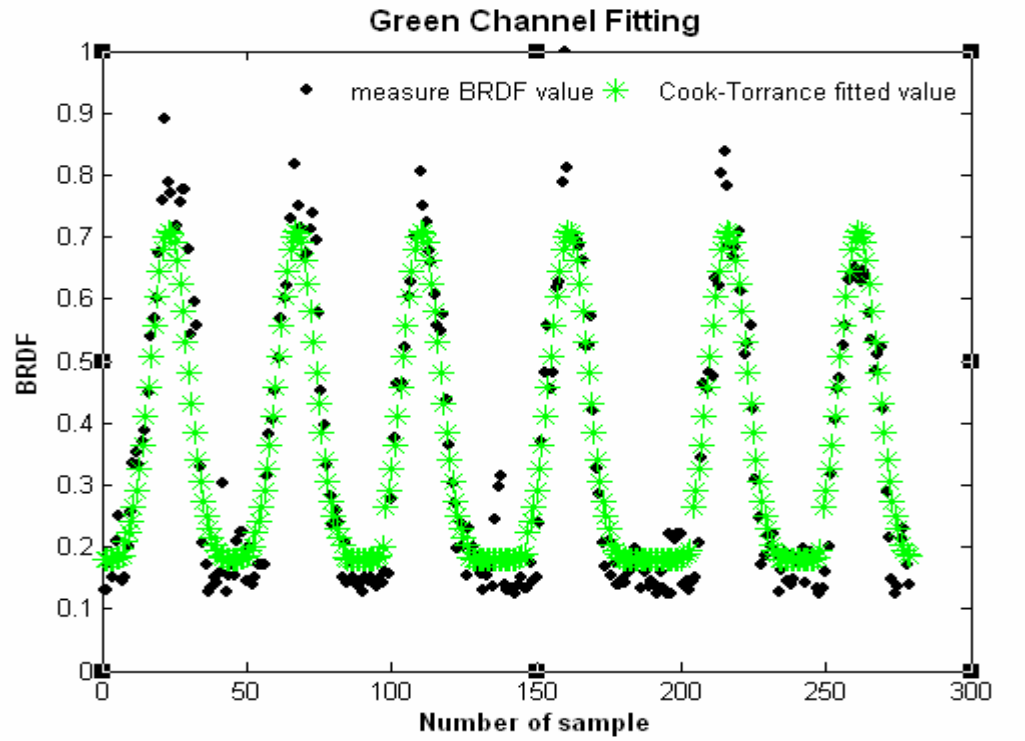

Figure 5.1b: Sample green channel fitting result for gold coated hemisphere sample.

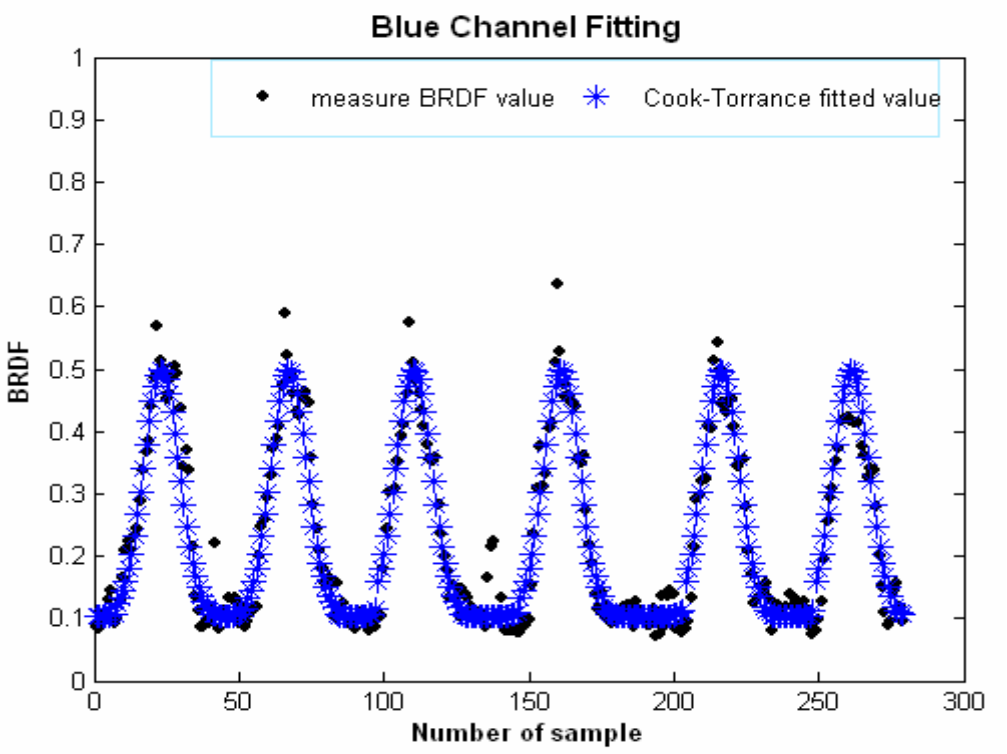

Figure 5.1c: Sample blue channel fitting result for a gold coated hemisphere sample.

Parameters	k_d	k_s	p_0 (=F)	p_1(=m)	SNR
Red channel	0.031	0.1454	0.303	0.1734	11.08
Green channel	0.031	0.0878	0.565	0.1734	11.02
Blue channel	0.016	0.2908	0.11	0.1752	11.04

Table 5.1: Fitted Cook-Torrance parameters for figure 5.1a, 5.1b and 5.1c. For Cook-Torrance Model, variable parameters are F and m.

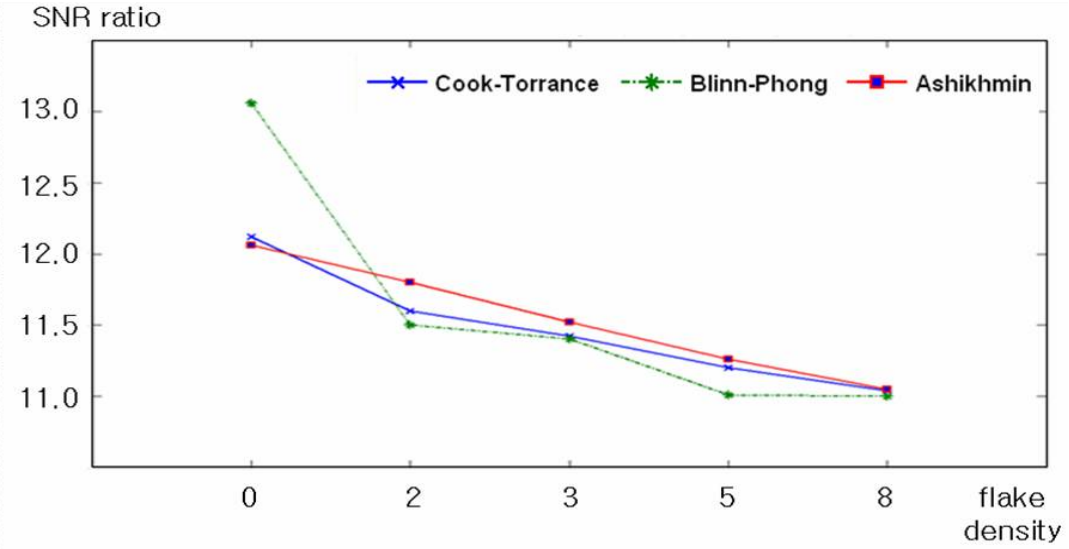

Figure 5.2: Sample figure for microstructure-based BRDF model fitting comparison

Figure 5.2 show that the density variation of flake, a microstructural component of coating material, affects the fitting performance of the BRDF models. When flake density of a coated surface increases while keeping the composition of other components same, the Signal-to-Noise (SNR) ratio of every model decreases. In our other fitting analysis, it shows that when the average flake size of coating microstructure increases while keeping the composition of other components the same, the SNR ratio also decreases. The most probable reason for these phenomena is that none of the existing BRDF models take account of the effect of microstructural composition on the appearance of coated surfaces. In addition, this microstructure-based comparison suggests that Ashikmin et al. [1] model performs the best among the three models presented in the figure in terms of SNR ratio. The fitting capability of Blinn-Phong and Cook-Torrance models for coated samples are almost same which contradicts the result of Ngan et al. [22], who evaluated the performance of several popular BRDF model in terms of their ability to fit measured data for 100 types of materials, found that Cook-Torrance and Ashikhmin et al. model perform the best in most cases. Our comparison shows that the performance of Cook-Torrance and Ashikhmin et al. model is almost same for solid or conventional paint i.e. when there is no flake in their microstructure (0% flake density). However, for other cases, the performance of Ashikhmin model outweighs that of Cook-Torrance BRDF model.

5.2 Rendering Result

We present the rendering results of microstructure-based modeling of the appearance of the coated surfaces in this section. We use a *MP3 player* and *Stanford Bunny* model for that purpose. We render these two models with coatings having varying composition of microstructure. Though, we have used gold and silver coating for our fitting and analysis purposes, we only show the rendering result of gold coating i.e. coatings with gold color here. We first render gold coated *Stanford Bunny* or *Mp3 Player* model with acquired BRDFs, measured by the image-based measurement system. To validate the fitting result, we also render the same model with Blinn-Phong, Cook-Torrance and Ashikhmin et al. analytical BRDF model with their respective fitted parameters.

Figure 5.3 shows the rendering results of *MP3 player* with measured BRDFs of gold coating having different flake density in its microstructure keeping average flake size same. The flake density of the rendering result increases from 0% to 8%. We can see from the results how the appearance changes when the flake density changes keeping all other composition of microstructure same. The rendering results *Stanford Bunny* model with measured BRDFs of gold coating having varying flake size in its microstructure is shown in figure 5.4. The composition of other components of these result are same and the density of flake is 8% in its microstructure.

In figure 5.5 and 5.6, we compare the rendering results of *Stanford Bunny* model based on measured data with the results based on three BRDF models using their respective fitted parameters. We can see from those figures that, for most of the case, Ashikhmin et al. model can best approximate the appearance with real measured data while Cook-Torrance and Blinn-Phong shows discrepancies. It is because the fitting performance of Ashikhmin et al. model is better than others as we have seen in fitting analysis. Though Ashikhmin model shows best performance in terms of approximating the appearance of the coated samples, there is subtle discrepancy with measured rendering results. We believe this is caused because none of the existing BRDF models presented in this thesis including Ashikhmin take the consideration of microstructural components of coating. Therefore, building a reflection model which will take consideration of the microstructural composition is a major challenge.

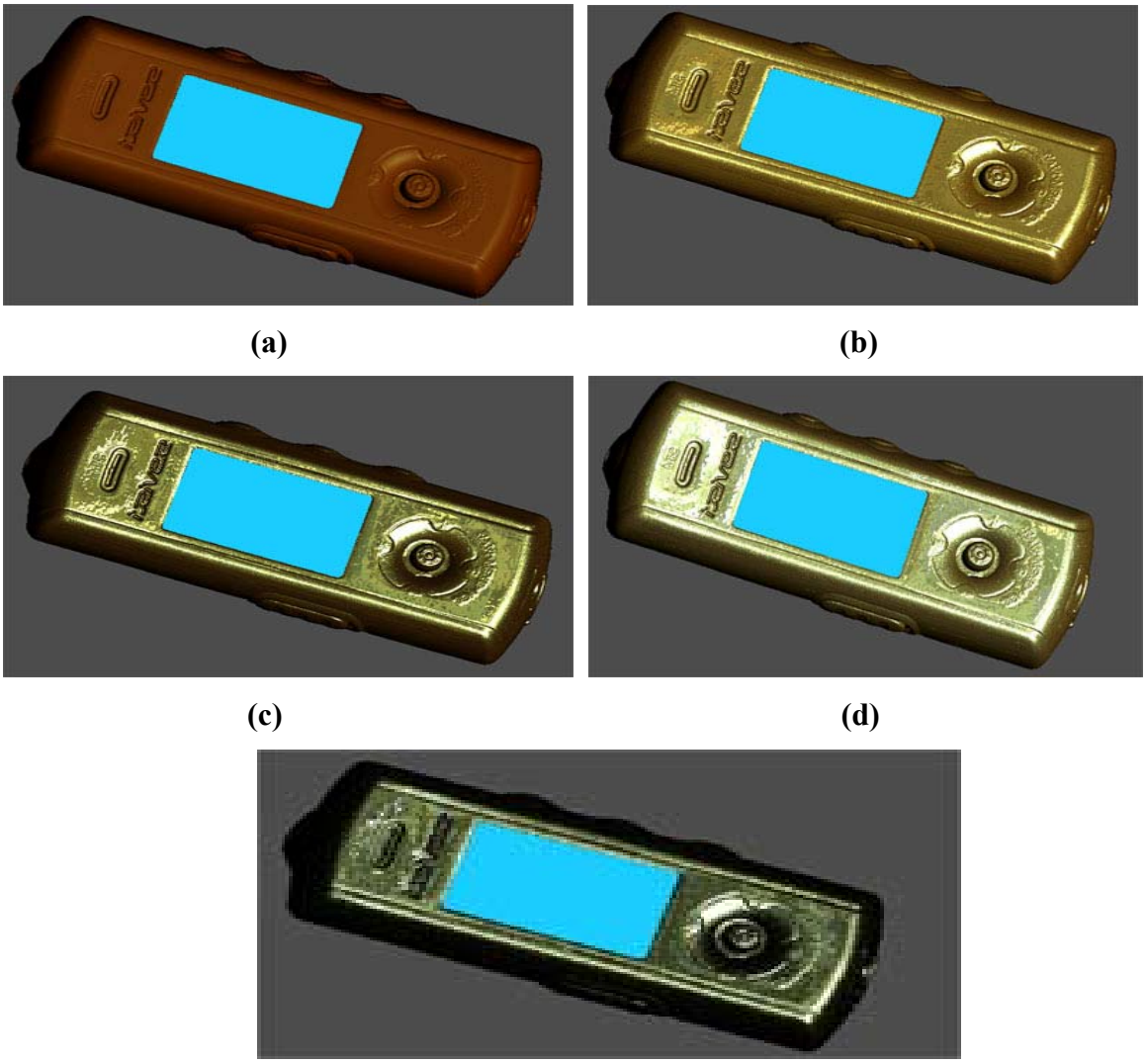

(a) **(b)**

(c) **(d)**

(e)

Figure 5.3: Rendering results of an *MP3 Player* with measured BRDFs for gold coating having flake density, from (a) to (e) 0%, 2%, 3%, 5% and 8% respectively. The compositions of other components are same in the microstructure of the coating with average flake size 25 microns.

(a) **(b)** **(c)**

Figure 5.4: Rendering results of *Stanford Bunny* model with measured BRDFs for gold coating having flake size, from (a) to (c) 15, 20 and 25 microns respectively. The compositions of other components are same in the microstructure of the coating with flake density of 8%.

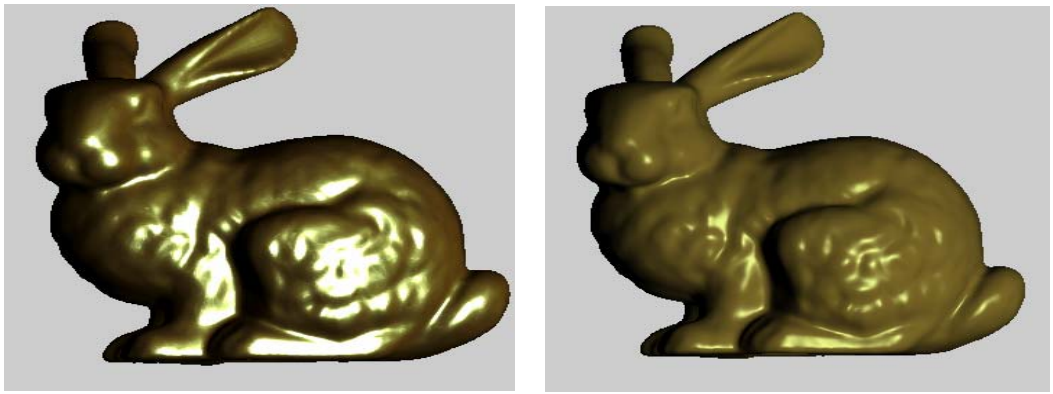

(a) **(b)**

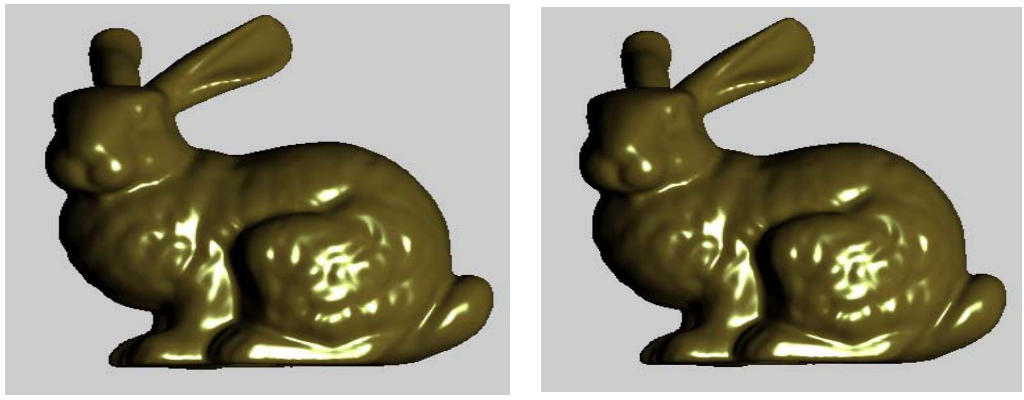

(c) **(d)**

Figure 5.5: Rendering results of *Stanford Bunny* with BRDF model for gold coating having 5% flake density in the microstructure of the coating with average flake size of 25 microns. Figure 5.5a shows rendering result with reference or measured BRDFs; 5.5b and 5.5c shows rendering result with the fitted parameters of Cook-Torrance and Ashikhmin et al. models respectively.

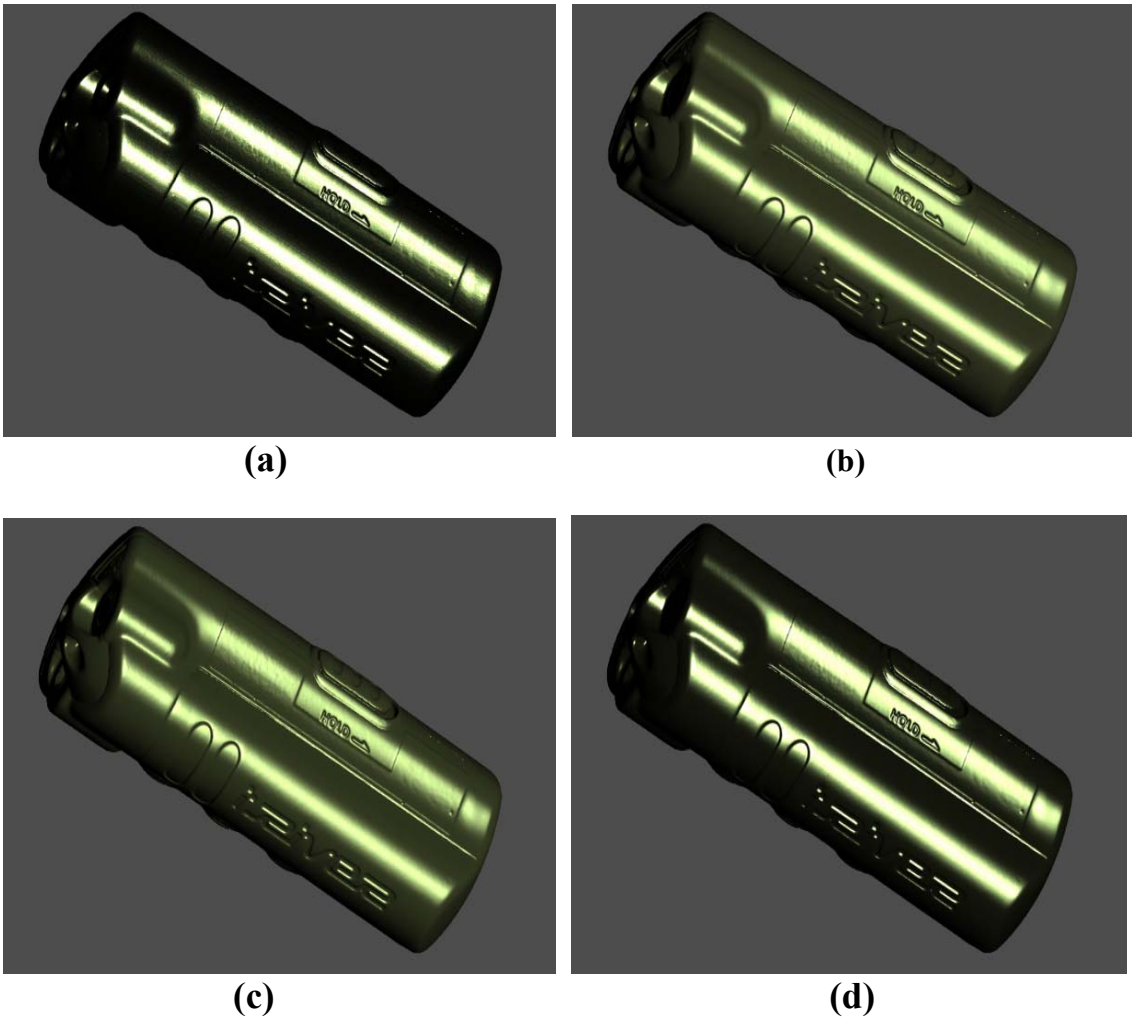

Figure 5.6: Rendering results of an *MP3 Player* with BRDF model with coating having 8% flake density in the microstructure of the coating with average flake size of 15 microns. Figure 5.6a shows rendering result with reference or measured BRDFs; 5.6b, 5.6c and 5.6d shows rendering result with the fitted parameters of Blinn-Phong, Cook-Torrance and Ashikhmin et al. models respectively.

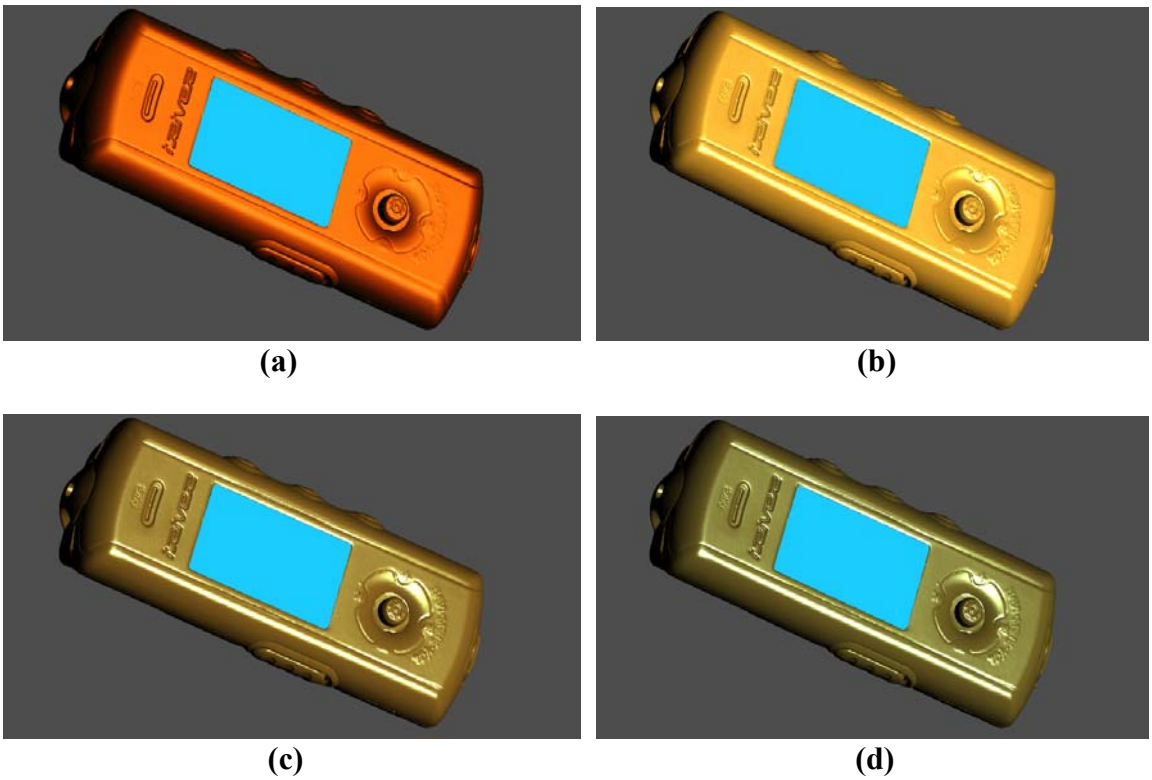

Figure 5.7: Rendering results of an *MP3 Player* with gold coating using Ashikhmin BRDF model. The flake density varies from (a) to (e) 0%, 2%, 3%, 5% and 8% respectively. The compositions of other components are same in the microstructure of the coating with average flake size 25 microns.

From the rendering and fitting result, we can conclude that Ashikhmin model is the best model among the existing BRDF models in terms of their ability to approximate the reflectance of coated surfaces and it can serve as a basis for building a new simple and easy-to-use reflection model which will take consideration of microstructural components' effect on the appearance for coated surface.

5.3 Chapter Summary

In this chapter, we have presented the results of microstructure-based modeling of coated surfaces. We have analyzed the performance of three analytical BRDF models by their ability to fit real measured BRDFs. Our experimental results suggest that Ashikhmin et al. model perform well for most the BRDFs of coated samples varying in their microstructural composition. Moreover, our results show that the performance of Blinn-Phong and Cook-Torrance model are almost same and cannot accurately model real BRDFs of coated surfaces. Our rendering result illustrate that a slight variation in the microstructural composition affects the appearance of coated surfaces. From the fitting and rendering result, it is obvious that there is a need of building a simple and easy-to-use reflection model that will be able to simulate the variation in appearance of coated surfaces which the slight variation of its microstructural composition entails and our best-performed Ashikhmin et al. model can serve as a basis for that model.

Chapter 6

Conclusions and Future Work

6.1 Conclusions

In this dissertation, we have introduced the microstructure-based modeling of coated surfaces. We first conduct a series of studies on the composition and different components of coating microstructure and how the components of coating microstructure influence the appearance of coated surfaces. These studies show that the composition of coating microstructure affects its appearance greatly, which we presented in chapter three. We modeled the appearance of coated surfaces that the variation of coating microstructure entails by a hybrid approach: using measured reflectance data as well as several analytical BRDF models whose parameters are determined by fitting the models to the real measured BRDFs of hemisphere-shape samples coated by professional painting studio. We have presented the rendering results of this hybrid approach in chapter 5. In addition, we analyzed three BRDF models in terms of their abilities to fit the measured BRDFs of coated sphere samples. Our analysis and rendering results suggest that physically-based Ashikhmin et al. [1] model performs better than other models for most of the fitting and rendering results of coated samples varying in their microstructural composition. Moreover, our results show that the performance of Blinn-Phong [3] and Cook-Torrance [5] model are almost same and cannot accurately model real BRDFs of coated surfaces. Our results also illustrates that, though Ashikhmin et al. model shows best performance in terms of approximating the appearance of the coated samples, there is still subtle discrepancy with measured rendering results. We believe this is caused because none of the existing BRDF models presented in this thesis including Ashikhmin et al. take the consideration of microstructural components of coating. Since the existing models have limitations in accurately representing some materials, there is a need to build a new a simple and easy-to-use reflection model which will take account of the presence of microstructural composition and ensure the explicit modeling of the microstructure-based BRDFs of coated surfaces.

6.2 Future Work

We believe that the work presented in this dissertation will stimulate more research in the field of microstructure-based modeling of coated surfaces. The most obvious extension of this dissertation is to build a simple and easy-to-use reflection model for the coated surface which will be able to explicitly simulate the variation in their appearance according to their composition of microstructure. We believe our best-performed Ashikhmin et al.'s BRDF model and data-driven model of Matusik et al. [20] can serve as the basis model for this work. Another extension of our work is microstructure-based modeling of more complex surfaces which have more than one layer in their microstructure and then building a reflection model for that surface.

We have used image-based measurement technique to acquire the BRDFs of coated samples. But, this technique has some drawbacks. This acquisition system is very complex and the preparation of the measurement target and the calibration involved is very tedious. The development of a portable and easy-to-use reflectance scanner is a major challenge.

The most promising research direction in the area of appearance modeling is the measurement and reproduction of spatially-varied material. Only very few objects in the real word are spatially homogeneous. As a result, even a perfect reproduction of the true BRDF only provides limited realism in a rendered scene. Moreover, while plenty of analytical models exist for BRDFs, there is exactly none for spatially-varying reflectance. Therefore, building a reflection model to approximate the reflectance of spatially varying material is another major future work.

BIBLIOGRAPHY

[1] M. Ashikhmin, S. Premoze, and P. Shirley. A microfacet-based BRDF generator. In *Proceedings of the 27th annual conference on Computer graphics and interactive techniques*, pages 65-74. ACM Press/Addison-Wesley Publishing Co., 2000.

[2] M. Ashikhmin and P. Shirley. An anisotropic phong BRDF model. *J. Graph Tools*, 5(2):25-32, 2000.

[3] J. F. Blinn. Models of light reflection for computer synthesized pictures. In *Proceedings of the 4th annual conference on Computer graphics and interactive techniques*, pages 192-198. ACM Press, 1977.

[4] M. Colbert, S. Pattanaik, and J. Krivanek. BRDF-shop: Creating physically correct bidirectional reflectance distribution functions. *IEEE Computer Graphics Application*, 26(1): 30-36,2006.

[5] R. L. Cook and K. E. Torrance. A reflectance model for computer graphics. In *Proceedings of the 8th annual conference on Computer graphics and interactive techniques*, pages 307-316. ACM Press, 1981.

[6] A. Duer. On the Ward model for global illumination. Submitted for review, Sept. 2004.

[7] P. Dumont-Bècle, E. Ferley, A Kemeny., S. Michelin and D. Arquès. Multi-texturing approach for paint appearance simulation on virtual vehicles, *In Proceedings of the Driving Simulation Conference*, Sophia Antipolis, pages 123-133, September 2001.

[8] S. Ershov, K. Kolchin and K. Myszkowski. Rendering Pearlescent Appearance based on Paint-Composition Modeling, In Proceedings of EUROGRAPHICS 2001, pages 227-238, September 2001.

[9] M. Goessele, H. P. A. Lensch, J. Lang, and H. –P. Seidel. Disco: Acquisition of translucent objects. *ACM Trans. Graph.*, 23(3):835-844, 2004.

[10] M. Goessele. New Acquisition Tecniques for Real Objects and Light Sources in Computer Graphics. Ph.D Dissertaion. Max-Planck Institute for Informatik, Germany, 2004.

[11] J. Günther, T. Chen, M. Goesele, I. Wald, and H. P. Seidel: Efficient Acquisition and Realistic Rendering of Car Paint, *In Proceedings of Vision, Modeling, and Visualization*, pages 487–494, 2005.

[12] X. D. He, K. E. Torrance, F. X. Sillion, and D. P. Greenberg. A comprehensive physical model for light reflection. In *Proceedings of the 18th annual conference on Computer graphics and interactive techniques*, pages 175-186. ACM Press, 1991.

[13] J. Heuberger and W. Pasman. Data Fitting Report. *Delft University of Technology* (2005).

[14] J. T. Kajiya. The Rendering Equation. In Computer Graphics (SIGGRAPH'86 Proceedings), 20(4):143-150, August 1986.

[15] E. P. F. Lafortune, S. –C Foo, K. E. Torrance, and D. P. Greenberg. Non-linear approximation of reflectance functions. *IEEE Transactions on Visualization and Computer Graphics*, 3(4):329-336, 1997.

[16] H. Lensch, M. Goesele, Y. –Y. Chuang, T. Hawkins, S. Marchner, W. Matusik and G. Mueller. Realistic Materials in Computer Graphics. In Siggraph 2005 tutorials. Los Angles, California.

[17] D. W. Marquardt. An algorithm for least-square estimation of nonlinear parameters, Journal of the Society for Industrial and Applied Mathematics, 11(1963): 431-441.

[18] S. Marschner. Inverse Rendering for Computer Graphics. Ph. D Dissertaion, *Cornell University*, Ithaca, NY, 1998.

[19] S. Marchner, S. Westin, E. Lafortune, and K. Torrance. Image-based measurement of the Bidirectional Reflection Distribution Function, *Applied Optics* 39(2000), no. 16, 2592-2600.

[20] W. Matusik, H. Pfister, M. Brand, and L. McMilan. A data-driven reflectance model. *ACM Trans. Graph.*, 22(3):759-769, 2003.

[21] W. Matusik. A Data-Driven Reflectance Model. Ph.D Dissertation, *Massachusetts Institute of Technology*, 2006.

[22] A. Ngan, F. Durand, and W. Matusik. Experimental analysis of BRDF models. In *Proceedings of the Eurographics Symposium on Rendering,* pages 117-126. Eurographics Association, 2005.

[23] A. Ngan. Acquisition and Modeling of Material Appearance. Ph.D Dissertation, *Massachusetts Institute of Technology*, 2006.

[24] F. Nicodemus, J. Richmond, J. Hsia, I. Ginsberg, and T. Limperis. Geometric considerations and nomenclature for reflectance. Monograph 160, National Bureau of Standards (US), October 1977.

[25] L. Neumann, A. Neumann, and L. Szirmay-kalos. Compact metallic reflectance models. *Computer Graphics Forum*, 18(13), 1999.

[26] M. Oren and S. K. Nayar. Generalization of lambert's reflectance model. In *Proceedings of the 21st annual conference on Computer graphics and interactive techniques*, pages 239-246. ACM Press, 1994.

[27] B. T. Phong. Illumination for computer generated pictures. *Communications of ACM*, 18(6):311-317, 1975.

[28] P. Poulin and A. Fournier. A model for anisotropic reflection. *Computer Graphics*, 24(4):273-382, Aug. 1990.

[29] W. H. Press, W. T. Vetterling, S. A. Teukolsky, and B. P. Flannery. Numerical Recipes in C++: the art of scientific computing. *Cambridge University Press*, 2002.

[30] M. Ramasubramanian, S. N. Pattanaik, and D. P. Greenberg. A perceptually based physical error metric for realistic image synthesis. In *Proceedings of SIGGRAPH 99*, pages 73-82, Aug. 1999.

[31] M. A. Robertson, S. Borman, and R. L. Stevenson. Estimation-Theoretic Approach to Dynamic Range Enhancement using Multiple Exposures. *J. Electronic Imaging*, 12(2):219-285, 2003.

[32] H. Rushmier, G. J. Ward, C. Piatko, P. Sanders, and B. Rust.Comparing real and synthetic images: some ideas about metrics. In P. M. Hanrahan and W. Purgathofer, editors, *Rendering Techniques '95*, Eurographics, pages 82-91. Springer-Verlag Wien New York, 1995.

[33] S. Rusinkiewicz. New change of variables for efficient BRDF representation. In G. Drettakis and N. Max, editors, *Rendering Techniques '98*, Eurographics, pages 11-22. Springer-Verlag Wien New York, 1998.

[34] S. Rusinkiewicz and S. Marchner. Measurement I – BRDFs. Script of Course CS448C: Topics in Computer Graphics, held at Stanford University, October 2000.

[35] C. Schlick. An inexpensive BRDF model for physically-based rendering. *Computer Graphics Forum*, 13(3):233-246, 1994.

[36] M. M. Stark, J. Arvo, and B. Smits. Barycentric parameterizations for isotropic brdfs. *IEEE Transations on Visualization and Computer Graphics*, 11(2):126-138, 2005.

[37] X. Tong, J. Wang, S. Lin, B. Guo, and H. –Y. Shum. Modeling and rendering of quasi-homogeneous materials. *ACM Trans. Graph.*, 24(3):1054-1061, 2005.

[38] K. Torrance and E. Sparrow. Theory for off-specular reflection from roughened surfaces. *Journal of Optical Society of America*, 57(9): 1105-1114, September 1967.

[39] I. Wald. Realtime Ray Tracing and Interactive Global Illumination. PhD thesis, *Saarland University*, 2004.

[40] G. J. Ward. Measuring and modeling anisotropic reflection. In *Proceedings of the 19th annual conference on Computer graphics and interactive techniques*, pages 265-272. ACM Press, 1992.

[41] Z. Zhang. A flexible new technique for camera calibration. *IEEE Trans. Pattern Anal. Mach. Intell.*, 22(11):1330-1334, 2000.